Patrícia Alexandra Dias Nunes

Bachelor of Chemical and Biochemical Engineering Sciences

Linking Process, Product and Performance by Raman Imaging Analysis

Dissertation submitted in partial fulfillment
of the requirements for the degree of
Master of Science in Chemical and Biochemical Engineering

Advisers: Ana Mafalda Gouveia de Paiva, MSc, Hovione
Pedro Manuel da Silva Cardoso Isidro Valente, PhD, Hovione

Co-advisers: Ana Isabel Nobre Martins Aguiar de Oliveira Ricardo, Full Professor, FCT NOVA

Examination Committee:

Chairperson:

Rapporteurs:

FACULDADE DE CIÊNCIAS E TECNOLOGIA
UNIVERSIDADE NOVA DE LISBOA

September 2018

Linking Process, Product and Performance by Raman Imaging Analysis

To my heroines on earth and my hero in heaven.

"The ultimate measure of a man is not where he stands in moments of comfort and convenience, but where he stands at times of challenge and controversy."

Martin Luther King Jr.

Acknowledgments/ Agradecimentos

Em primeiro lugar quero agradecer à Faculdade de Ciências e Tecnologia da Universidade Nova de Lisboa pelo excelente percurso curricular proporcionado. Quero também agradecer à Hovione FarmaCiência por me ter dado a oportunidade de estagiar durante seis meses numa empresa de renome e muito valor. Quero agradecer imenso aos meus orientadores na Hovione. Um enorme obrigada ao Pedro Valente por me ter incutido o gosto pela programação, por me ter motivado e por ter valorizado sempre a minha eficiência já que "An apple doesn't fall far from the tree". Um enorme obrigada à Mafalda Paiva por todo o apoio, todo o pensamento positivo transmitido e por confiar no meu trabalho. Um obrigado à professora Ana Aguiar Ricardo por ter dado um apoio extra e por ter sempre sugerido melhorias ao meu trabalho. Um enorme obrigada às pessoas que de alguma forma contribuíram para o trabalho que realizei no laboratório. Obrigada à Teresa pela ajuda nas análises de performance, à Raquel pela ajuda no *XRPD* e um grande obrigado ao André e ao Calixto pelos ensinamentos sobre *spray drying* e *tableting*. Um obrigado à Célia por me animar todas as manhãs com um sorriso e um galão. Obrigada a todos os alunos da Sala Eureka que contribuíram sempre com algo de bom para o meu estágio nestes seis meses. Obrigada Tiago pelo *bullying* e pela compreensão no que toca à frustração com programação, obrigada Bruno pelos momentos de exploração do Raman, obrigada Beatriz por me escolheres sempre como tua motorista, obrigada António por quebrares a minha atenção quando eu precisava de me distrair e um obrigada muito especial à minha companheira de escrita e amiga nos tempos livres (que são poucos) Mariana Fernandes.

Quero agradecer à minha irmã e à minha mãe que me apoiam em tudo, dando-me força nos momentos mais críticos e principalmente inspirando-me sempre com a garra e determinação que nos está no sangue. Um muito obrigado ao meu cunhado que me faz sempre pensar nos meus objetivos e que também me inspira a fazer sempre melhor. Um enorme agradecimento ao João por estar sempre ao meu lado no melhor e pior, por me ter motivado em momentos mais difíceis e por ser das poucas pessoas que me põe um sorriso na cara em momentos nos quais sorrir é o que menos me apetece fazer. Obrigada à melhor *team* que tive na minha vida toda: "Team Projeto", os quais estiveram sempre ao meu lado na procrastinação e no trabalho, na alegria e na tristeza e nem o Erasmus nos separou. Bruno, obrigada por me teres ensinado a gostar de um grupo de pessoas mais restrito. Kets, obrigada por testares a minha paciência ao limite todos os dias, isso deu-me ferramentas muito importantes para aplicar no futuro. Gonçalo, obrigada por seres tu: feliz e inspirador e por todas as horas de conselhos trocados. Por fim, mas não menos importante, obrigada aos "Amiguinhos do Zalves" e aos "Miguxos" por animarem os meus dias sempre com temas interessantes sobre a atualidade e por terem feito destes cinco anos os melhores anos da minha vida.

Abstract

This work aims at exploring two applications of Raman spectroscopy in the development and manufacturing of pharmaceutical tablets made from amorphous solid dispersions (ASDs), in terms of both physical and chemical properties.

The first application consisted on applying Raman spectroscopy to predict the tablets' hardness. In contrast to typical destructive hardness testing, this strategy can be implemented as at-line and real-time process control via process analytical technology and thus provide real-time release during continuous manufacturing. This is investigated here for the first time for tablets composed of ASDs rather than crystalline-based formulations using a Confocal Raman Microscope. The generated data show an apparent relationship between the measured hardness and the Raman spectra baseline, consistent with previous findings in the literature. However, a more stringent analysis leads to the conclusion that the trend line is not strictly monotonic and with a slope across the measured range comparable to the variability of the Raman imaging analysis.

The second application consisted on exploring the potential of confocal Raman microscopy to provide spatially resolved chemical images of the tablets' surface, which allows to characterize the components spatial distribution. The goal was to evaluate the impact of two process parameters: blending shear rate and sieving mesh size. These parameters were investigated using a structured 2-level design of experiments where Confocal Raman microscopy allowed the evaluation of the spatial distribution and the detection of API agglomerates and its relationship with the process parameters. However, the analysis was hindered by a lack of a perfectly flat surface of the tablets and to correct the influence of the change in focus on the Raman spectra, post-processing scripts were implemented. It is shown that there is an impact of both process parameters on the heterogeneity of tablets' surface and, consequentially, a significant impact in disintegration of the tablets.

Keywords: Confocal Raman Imaging, Pharmaceutical Technology, Process Development, Continuous Manufacturing

Resumo

Este trabalho tem como objetivo perceber o potencial da espectroscopia de Raman para a caracterização de propriedades físicas e químicas de comprimidos produzidos a partir de uma dispersão sólida amorfa durante o desenvolvimento e produção dos mesmos.

O primeiro estudo consiste na aplicação da espectroscopia de Raman na medição da dureza de comprimidos. Esta técnica pode ser utilizada em linha e permite o controlo do processo em tempo real, permitindo a libertação de lotes em tempo real durante produção contínua. Este é o primeiro estudo que utiliza um microscópio confocal de Raman para caracterizar a dureza de comprimidos feitos por dispersões sólidas amorfas em vez de formulações baseadas em formas cristalinas. Os resultados são comparáveis à literatura existente, pois mostram uma possível relação entre a dureza medida por testes destrutivos e a linha de base do espectro de Raman. No entanto, o declive da linha de tendência tem um valor muito baixo e comparável à variabilidade dos dados da mesma experiência.

O segundo caso de estudo consiste em perceber o potencial da microscopia confocal de Raman para caracterizar a distribuição espacial dos componentes à superfície dos comprimidos. O objetivo é avaliar o impacto da agitação da mistura e do tamanho do peneiro na homogeneidade dos comprimidos. Para isso, foi planeado um desenho de experiências no qual ambos os parâmetros foram variados a dois níveis e a distribuição espacial dos componentes foi avaliada usando a microscopia confocal de Raman. Não sendo a superfície dos comprimidos perfeitamente plana, foi necessário tratar os dados obtidos para corrigir a influência dos problemas de foco. Os resultados mostraram que ambos os parâmetros de processo têm impacto na heterogeneidade da superfície dos comprimidos e consequentemente têm impacto na desintegração dos mesmos.

Palavras-chave: Microscopia Confocal de Raman, Tecnologia Farmacêutica, Desenvolvimento de Processo, Produção Contínua

Table of Contents

List of Figures

List of Tables

List of Acronyms

AFM	Atomic Force Microscopy
API	Active Pharmaceutical Ingredient
APS	Amorphous Phase Separation
ASD	Amorphous Solid Dispersion
CARS	Coherent Anti-Stokes Raman Scattering
CCDs	Charged-Coupled Devices
CM	Continuous Manufacturing
CRM	Confocal Raman Microscopy
DCM	Dichloromethane
DoE	Design of Experiments
DSC	Differential Scanning Calorimetry
EMA	European Medicines Agency
FDA	Food and Drug Administration
FT-Raman	Fourier Transform Raman Scattering
FT-SERS	Fourier Transform Surface-Enhanced Raman Scattering
HCl	Hydrochloric Acid
HPMC	Hydroxypropyl Methylcellulose
HPMCAS	Hydroxypropyl Methylcellulose Acetate Succinate

ICH	International Conference on Harmonization
IR	Infrared
mDSC	Modulated Differential Scanning Calorimetry
MeOH	Methanol
NA	Numerical Aperture
NIR	Near-Infrared
PAT	Process Analytical Technology
PMTs	Photomultiplier Tubes
rpm	Rotations per minute
RR	Resonance Raman Scattering
SDD	Spray Dried Dispersion
SERRS	Surface-Enhanced Resonance Raman Scattering
SERS	Surface-Enhanced Raman Scattering
SNR	Signal-to-noise Ratio
TGA	Thermogravimetric Analysis
USP	United States Pharmacopeia
XRPD	X-Ray Powder Diffraction

1

Introduction

1.1 Motivation

In the pharmaceutical industry there has been an increasing interest in continuous manufacturing (CM) since it is a more productive and safer production method. Continuous manufacturing also enables better quality control of the final products. An example of this interest is the Novartis-MIT Center for Continuous Manufacturing, as the center develops new technologies to replace the pharmaceutical industry's conventional batch-based system with a continuous manufacturing process [1]. The CM also enables higher yields and productivity due to reduced non-productive down-time and reduced cycle time by avoiding vessel heat-up or cooldown times or downtime associated with charging and emptying of materials. These advantages together with the increased energy efficiency and reduced solvent consumption lead to a higher economic viability. Additionally, CM can provide added safety as it can prevent cross-contamination once there is no need to transfer the intermediate products between the unit operations.

One such application of continuous manufacturing in the pharmaceutical industry has been the downstream processing of pharmaceutical powders into a final dosage form such as an oral tablet. In tableting manufacturing, production starts when the crystalline or amorphous active pharmaceutical ingredient (API) system is sieved and blended with excipients, depending on the final product application. The excipients can have many applications such as API stabilization, flowability enhancement [2], disintegration, solubility and bioavailability enrichment [3], [4]. The overview of the unitary operation involved in the production of a pharmaceutical tablet is presented in Figure 1.1 [5], [6]. Often, after tableting, the oral dosage forms are coated for aesthetic purposes or to enhance the performance of the tablets for a specific application, for example enteric coating [7].

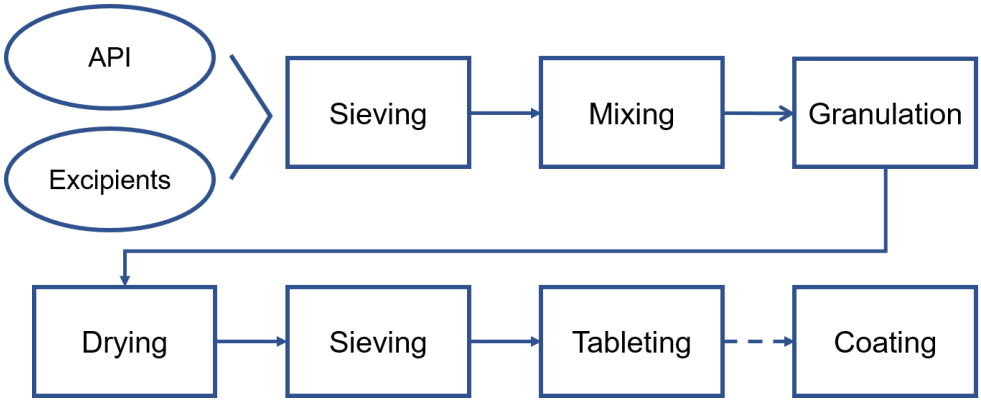

Figure 1.1 - Schematic Representation of Tablets' Production (The figure was adapted from [6]**)**

For pharmaceutical drugs in the development pipeline which exhibit poor water solubility, a solubility enhancement platform is often necessary to ensure the drug's bioavailability. Formulating the API as an amorphous solid dispersion (ASD) is one of the most popular and effective solubility enhancement approaches. The ASD is based on the integration of an amorphous drug in a glassy polymer matrix. ASDs can be produced using hot melt extrusion resulting in a extrudate or by solvent evaporation, typically by spray drying resulting in a spray-dried dispersion (SDD) [8].

Process Analytical Technology

Every development step requires quality control and the control is usually performed by destructive methods that also need sample preparation as assay, bulk and content uniformity [9]. For CM to be viable, however, there must be a real-time quality control. It can be provided by continuously monitoring via process analytical technology (PAT) which is able to make real-time adjustments to maintain the quality parameters of both intermediate and final products [10].

Jukka has defined process analytical technology as: a system for developing and implementing new efficient tools for use during pharmaceutical development, manufacturing for quality assurance while maintaining or improving the current level of product quality assurance [11].

The regulatory agencies have encouraged the pharmaceutical industries to apply PAT tools to improve the quality assurance in continuous manufacturing. For example, the European Medicines Agency (EMA) established a PAT team in 2003 [12] and the Food and Drug Administration (FDA) issued ‘‘Process Analytical Technology - Guidance for Industry’’ on September 2004 which highlights PAT to have appropriate in-process quality control while manufacturing [13]. The Q8, Q9, Q10 and Q11 guidelines published by International Conference on Harmonization (ICH) [12], [14], [15] and “Good Manufacturing Practice”: Annex 15 and 17 by EMA are good examples of the absent of specific regulatory barriers to continuous manufacturing [14].

The interest in using Raman Spectroscopy for quality assurance in pharmaceutical industries has also been increasing, with multiple examples of successful integration into real-time release test-

ing, continuous manufacturing and statistical process control [12], [16]. Raman Spectroscopy allows non-destructive rapid analysis as it needs minimal or no sample preparation. This technique can be used in real-time process control since it provides high throughput for quality assurance [5], [12], [17], [18]. The potential of Raman spectroscopy as a PAT have been studied for chemical identification and quantification [18]–[20] and counterfeit analysis [21]. Raman has been described as a suitable technique to predict tablets physical properties [5], [15], [22]–[24] and to assure quality of coated tablets (e.g. coating thickness) [17], [25], [26]. Additionally, applications of Raman spectroscopy on quantification of amorphous conversion and phase separation have been described. This is a great advantage for ASDs' quality assurance, since the long-term stability of ASDs might be impaired by the recrystallization and/or amorphous phase separation (APS) [27]. Also, it is important given that a phase change of an API could impact in chemical and physical stability, shell life and bio-performance of the drug [18], [28].

In summary, the application of Raman spectroscopy and microscopy have been increased and the implementation of these techniques have occurred at different stages of drug discovery and development [29]. These techniques have been described as suitable for advanced characterization in terms of chemical identification, pre-formulation screening, spatial component distribution and counterfeit identification [30].

Considering the previous described applications and advantages of Raman spectroscopy and microscopy, this work aims at exploring the potentialities of Raman imaging to characterize final oral dosage forms (i.e. tablets), produced from ASDs in terms of physical and chemical properties. In terms of physical properties, Raman imaging will be applied to understand if there is a feasible correlation between Raman signal and tablets' hardness. Regarding the chemical characterization, Raman microscopy will be applied as an advanced technique to provide spatially resolved chemical maps. These chemical maps will provide information on spatial component distribution and assess possible heterogeneity at a micro-scale.

1.2 Raman Spectroscopy

The basic principal of Raman Spectroscopy is the Raman scattering, where a substance is irradiated with monochromatic light. The inelastic scattering of electromagnetic radiation by this substance, with a different frequency of the incident beam, is detected. The differences between the frequencies of these radiations result in characteristic Raman shifts [11], [16]. Raman scattering can be explained according to classical theory [31]–[33]. The molecule is irradiated by the external electric field (E) which is distorting the electron distribution of the molecule and inducing an electric dipole moment (μ). The proportionality constant is the molecular polarizability (α) which represents the ability of an external field to disturb the electron density of the sample from its equilibrium configuration.

$$\vec{\mu} = \alpha \vec{E} \quad \textbf{(1.1)}$$

The scattered photons can either gain (anti-Stokes scattering) or lose (Stokes scattering) energy from the molecules within the sample (Figure 1.2 [32], [33]. Both the scattered photons energies and the transitions' intensities provide the identification of the present molecules [34].

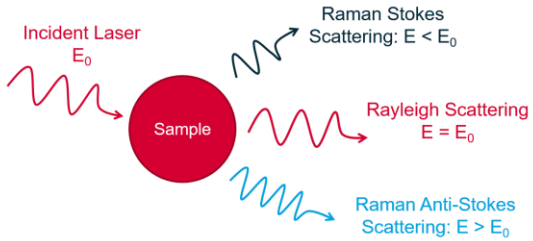

Figure 1.2 – Schematic Representation of Raman Scattering

The probability of Raman scattering occurring is $1{:}10^7$ scattering events. The Raman signal is weak when compared to emission techniques for which the probability is 1:10 photons and to near-infrared (NIR) spectroscopy that has a probability of $1{:}10^5$ photons [34]. The Rayleigh scattering has a probability of about 10^{-5} in 1 m of air, since the majority of scattered photons are elastic scattered [32], [34]. Comparing the two types of Raman scattering, the Stokes scattering is the most commonly represented in the Raman spectrum, since the anti-Stokes bands are less intense. This can be explained by the population of molecules present in the vibrational level v=1 being less than in the v=0. The population of molecules in each vibrational level is related to the energy between them (ΔE) by the Boltzmann distribution (Eq. (1.2)) [34].

$$\frac{N_{v=1}}{N_{v=0}} = \exp\left(\frac{-\Delta E}{k\,T}\right) \quad \textbf{(1.2)}$$

When compared to infrared (IR) spectroscopy, the disadvantages of Raman spectroscopy are the low probability of the Raman scattering and the fact that asymmetrical functional groups with a large dipole moment do not yield strong signals [33], [35]. However, this can also be seen as an advantage, since this is the reason why Raman yield very low water signals [33], [35] and thus it allows the sensibility for analyzing aqueous solutions. This is an advantage of Raman spectroscopy since it can be applied to follow reactions [36] and dissolutions [8], and to analyze biological cells [9]. Additionally, Raman is a better tool for polymorphic forms characterization, when compared to IR or NIR spectroscopy, since the vibrations originating from the crystal lattice (phonons) and from the carbon backbone yield much stronger signals in Raman. Also, the majority of the relevant information about solid-state is presented in low wavenumber region, which is easily accessible by Raman [33].

The first evidence of Raman Scattering was discovered by Chandrasekhra Venkata Raman in 1928. The energy source was the sunlight, a telescope was the collector and he detected this effect with his vision [32]. However, Raman Spectroscopy started to be a routine technique only after both the laser became a usual source of monochromatic electromagnetic radiation and the

commercially availability of dispersive laser Raman spectrometer, in 1969 [33], [37], [38]. In that time, photomultiplier tubes (PMTs) were used as point detectors. These detectors were only sensitive for a narrow range of wavelengths and the exit slit of the spectrometer selected this range. Then, in the 1970s and 1980s, the PMTs were replaced by charge-coupled devices (CCDs), enabling the detection of 1000 channels at the same time [33].

Since then, Raman spectroscopy has evolved with some advanced techniques [29], [39], such as: Fourier Transform Raman Scattering (FT-Raman) [40], [41], Resonance Raman Scattering (RR) [31], Surface-Enhanced Raman Scattering (SERS) [42] and Coherent Anti-Stokes Raman Scattering (CARS) [43]. The combination of some of these advanced techniques had been widely used in pharmaceutical context (e.g.: FT-Raman combined with SERS (FT-SERS), RR combined with SERS (SERRS)). The development of Raman spectroscopy continued, and this technique started to be combined with optical microscopes [31]–[33], [39], being this subject of great relevance to the present work.

1.3 Raman Microscopy

Raman spectrometers and microscopes have evolved with the advancements in photonics and optoelectronics, and the need for more information rather than the physical and chemical information leaded the way to Raman Microscopy [29]. This term corresponds to the combination of Raman Spectroscopy with an optical microscope, which was first developed in the 1990s. A great advantage of this combination is to use a microscope objective lens which provides higher collection efficiency due to the high numerical aperture (NA) [33].

Regarding the microscopy field, several techniques are used to characterize particle size, particle size distribution and morphology. The combination of microscopy with spectroscopy provides both spatial and chemical information on the ingredients within a formulation. This enables analyses such as sample homogeneity [30], [44], spatial distribution [19], [45], [46] and stability of the sample after exposed at high temperature and high humidity conditions [33], [47].

1.4 Confocal Raman Microscopy

The increase of nanotechnology and biotechnology applications leaded to the interest of studying systems that are at the micro and nanoscale. This interest has contributed to the creation of mechanisms of great resolution [39]. The need for spectroscopic techniques to evolve in this way is continuously increasing [37], [42].

Confocal Raman microscopy information has been described to provide essential information during pharmaceutical development in terms of drug substance design and development of liquid and solid formulations. This technique is also an important tool to assure process quality control as well [33]. The concept of confocal imaging was patented by Marvin Minsky, in 1957 [48] and a schematic representation of this mechanism is showed in Figure 1.3.

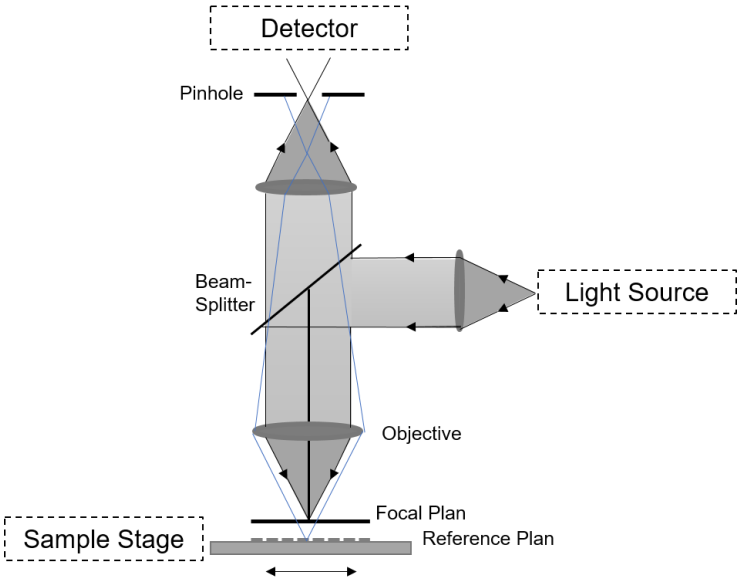

Figure 1.3 - Schematic Representation of Confocal Raman Microscopy (The figure was based on figures provided by [33], [39]**)**

In confocal Raman microscopy (CRM), the light (usually a laser) is focused onto the sample with the microscope objective lens. The backscattered light is refocused onto a pinhole aperture before reaching the detector. The small pinhole aperture blocks the background and out-of-focus light which do not correspond to the focal plane. The Raman signal detected by the spectrometer is dispersed using a CCD camera to generate the spectra. The sample stage is able to move the sample while performing the analyses, which enables analyses of two-dimensional images [33], [39]. Thus, confocal Raman microscopy provides high lateral and depth resolution, since the scattered light from above and below the focal plane does not contribute to the produced image [29], [33], [39]. Therefore, as CRM can axially discriminate signals originating from selective depth, images in depth can be performed (e.g. component distribution along different layers) [29]. The resolution varies between 1 and 100 µm. With this range of spatial resolution, large area scans can be performed and entire tablets can be characterized [33], and powder inhalation formulations with particle size below 10 microns can also be characterized.

The most common application of this tool is imaging of solid dosage forms to prove content uniformity [45] and study solid state [49]. Additionally, CRM can detect solid state changes in the API at the surface of the tablet, at least due to high temperature, humidity and mechanical stress. Concentrations below 1 %(w/w) are detectable and polymorphic impurities of only 0.05 %(w/w) were already described [19], [50]. In the amorphous solid dispersions field, CRM were found to evaluate phase separation [27], as well as to follow the release mechanisms of a poorly soluble drug from amorphous solid dispersions [8].

Considering these advantages, confocal Raman microscopy will be used in the present work to assess on the spatial distribution of compounds within tablets made from amorphous solid dispersions.

1.4.1 Critical Parameters

With the purpose of obtaining comparable results, the limitations of the equipment must be considered. Also, all the parameters that influence those limitations and can be controlled have to be set before the analyses. Parameters such as laser wavelength and laser power, spatial and temporal resolution are inherent to all Raman apparatuses [33]. Additionally, focus plane is an important parameter to consider while using a confocal Raman microscope [34].

Laser Wavelength and Laser Power

The irradiating laser wavelength and laser power must be chosen carefully. When a shorter wavelength is chosen, the sample can heat up when absorbing energy. Also, the sample can suffer decomposition, polymorph conversion or sample burning [33], [51]. The probability of sample heating is higher for smallest spot size (e.g. using a microprobe). This effect usually is a major problem for colored and highly absorbing species, or for small particles with lower heat transfer. These events can be observed either as changes in the Raman spectrum over time or by visual damage of the sample. [51]

Fluorescence is other possible effect to occur if the laser excitation wavelength overlaps with an absorption band of a fluorescent compound. This effect is usually observed as a broad sloping background underlying the Raman spectrum. Thus, fluorescence causes an increase in the baseline, which masks the peaks in the spectra and can also reduce the SNR [51], [52]. The fluorescence occurrence depends on the sample that is studied. A possible way to reduce this effect is to either use longer wavelengths excitation sources such as 785 nm or 1064 nm or reduce the intensity of the laser by reducing the laser power that is applied to the sample. However, Raman signal is proportional to $(\upsilon_0 - \upsilon_m)^4$, when υ_0 is the wavenumber of the excitation laser and υ_m is the wavenumber of the vibrational mode. Thus, for longer wavelengths, the fluorescence is less probable to happen, but also Raman signals are weaker when compared to shorter wavelengths [51]. Thus, the optimum laser power which maximize SNR, minimize black-body radiation and has not a significant fluorescence effect must be assessed [33]. The higher signal-to-noise ratio should be found by balancing fluorescence rejection, signal strength, and detector response [51].

Spatial Resolution

The spatial resolution corresponds to the size of the irradiated volume [34]. The resolution and the collection efficiency of the microscope are defined by the numerical aperture (NA) of the objective lens. Thus, the NA must be maximized, and this can be achieved with objectives with short working distance. However, to evaluate solid dosage forms such as tablets, objectives with long working distance are required (for example: 10x lens and 20x lens) [33]. The theoretical resolution limit of a microscope can be determined by the Abbe equation (Eq. (1.3)), which calculates the diffraction limited spot size [34].

$$d = \frac{\lambda}{2\,NA} \tag{1.3}$$

Raman microscopes usually have spatial resolutions below 1 µm [33], [39]. The microscope used in this work is a confocal Raman microscope equipped with a 532 nm laser wavelength. So, if a 100x objective lens with a NA of 0.9 would be used the limit spatial resolution would correspond to 296 nm.

The result provided by equipment is an averaged spectrum of the probe size. For example, in the microscope used in this work, if a 20x lens is used, the probe size is around 15 µm and for the 100x objective the probe size is ca. 3 µm. Thus, the step size between points should be smaller than the smallest spot size to perform an image scan. [53]. However, care must be taken while choosing the spatial resolution, to guarantee a resolved image but at the same time avoid overlapped spectra.

Another important parameter to determine is the image spatial resolution which corresponds to the quotient between image size and the number of points analyzed. For example, if an image of 1000 µm x 1000 µm size is analyzed by Raman microscopy with a large area scan of 200 x 200 points, the spatial image resolution is 5 µm. From this point forward, image spatial resolution will be called spatial resolution.

Temporal Resolution

With the purpose of maximizing the data signal quality, there are two additional parameters that must be set to use in all experiments: the acquisition time and the number of acquisitions of a spectrum. A spectrum is acquired during a certain acquisition time and a defined number of spectra are combined in an averaged spectrum. The acquisition time and the quality of the resultant spectra are directly correlated [33]. Lower accumulation time leads to a lower axial resolution, lower quality of the spectra and consequentially to blocky image [30].

In an industrial environment, the interest is to perform results as fast as possible. Thus, a compromise must be taken between these two parameters, to perform good results, measured by the signal-to-noise ratio (SNR), and fast results, depending on the timelines imposed.

Focus Plane

In this work, Confocal Raman Microscopy is used as an imaging technique. When using this type of confocal apparatuses, the Raman signal will be properly yield just in focused samples, as mentioned before. The sample in-focus and out-of-focus has different relative intensities of Raman peaks and this difference is a multiplicative factor, since the entire spectrum is affected in the same way [34]. Thus, the focus plane is an important parameter to be considered [33] and has been study by Helešicová *et al.* [30]. The middle focus level was found to be the most suitable position, since the most part of the sample area was focused, reflecting in the quality of Raman

maps. Also, if cross-sections are analyzed, the roughness is important to be considered and flat surfaces are preferred [30].

All these parameters should be considered while defining the analysis methodology, to obtain the higher data quality with the optimal analysis parameters using a confocal Raman microscope.

1.5 Hardness Characterization

The crushing strength is one of the critical quality attributes of final dosage forms such as tablets. This parameter has been determined using mechanical methods as diametral compression test, where an increasing force is applied on opposite sides of a tablet until crushing is obtained [54]. Currently, tablets' hardness is measured by destructive methods and there is a need to develop non-destructive and in-line methodologies.

The use of Raman spectroscopy to predict physical properties of tablets, such as crushing strength (i.e. hardness), friability, porosity and density has been studied in the literature [5], [15], [22]–[24].

Wang *et al.* described the variation of Raman intensity with the variation of tableting pressure, i.e. compression force divided by cross sectional area of tablets. Raman intensity decreased with the increase of tableting pressure until reached a plateau after ca. 350 MPa of tableting pressure [55]. In 2012, Heigl *et al*. supported this result, detecting an attenuated Raman scattering, for higher values of the tablets' hardness [24]. Contrarily, Virtanen *et al*. also used Raman spectroscopy to determine tablet's crushing strength and noticed an increase of the spectra baseline with the increasing of crushing strength [23].

In terms of tablets' density, Johansson *et al.* investigated the effect of tablet's density on the Raman assessment. The tablets' compression force was varied, and Raman spectroscopic analyses were performed using different irradiation patterns: point, circle and area irradiation. The results showed no significant effect of tablet's density on the Raman shifts intensities [22].

In 2006, a prediction model for pharmaceutical properties such as hardness and porosity, using directly raw data from Raman spectroscopy was successfully developed by Shah *et al.* [5]. However, recent studies were carried out by Peeters *et al.* (2016) to evaluate the impact of varying granulation parameters in physical properties of tablets (tensile strength, friability, porosity and disintegration time). In this study, the physical properties could not be predicted either by Raman or NIR spectroscopy [15].

Considering the previous literature, inconsistent results had been obtained for the prediction of physical properties by Raman spectroscopy. This discrepancy has been explained by differences in methodology, setup used and formulations studied.

The interest in obtaining a prediction model for tablet hardness by spectroscopy techniques continues, since currently tablet's hardness is determined by destructive methods that cannot be applied in-line, during continuous manufacturing. Also, the previous literature had only studied formulation made from crystalline APIs. Thus, this study aims at studying a possible correlation between Raman spectra and tablets' hardness produced from ASDs. Additionally, a confocal Raman microscope will be used.

1.6 Spatial Component Distribution

During pharmaceutical development, the interaction between the API and excipients is an important factor to be considered while testing several formulations. Thus, this interaction must be assessed in early stages of formulation design to move forward to oral dosage form production, with less risk of failure. Additionally, the variation of process parameters can influence the performance of the final product. Thus, advanced characterization is required to investigate the impact of these variations in the formulations.

Confocal Raman microscopy has been described as a suitable technique for advanced characterization since it provides high lateral and depth resolution [9]. CRM has been described to provide information on homogeneity of a sample, solid state of a component and the distribution of ingredients within a final drug product, such as tablets [33].

Breitenbach *et al.*, in 1999, described confocal Raman spectroscopy as an analytical approach to solid dispersions and mapping of drugs. In this study, Raman was proved to determine the amorphous state of ibuprofen in a solid dispersion and to characterize the homogeneity of the drug within a extrudate tablet [44]. Confocal Raman spectroscopy were employed by Scoutaris *et al.* to map the distribution on the surface of paracetamol tablets produced by direct compression, both qualitatively and quantitatively [46]. Also, Henson and Zhang exhibited the spatial API distribution of low content pharmaceutical tablets and presented this distribution in two ways: chemical images and histograms with the content distribution. Three forms of API were detected and spatially identified [19].

A more detailed description of the influence of different acquisition settings and the focus adjustment on Raman spectral maps of pharmaceutical tablets using CRM was described by Helešicová *et al.* The conclusions were that both CRM is a suitable technique to perform homogeneity studies and the type of analysis is the parameter that has the most influence on the quality of resultant images [30].

In terms of process parameters variation, Šašić compared spatial distribution of the five components of tablets from batches produced by two different methods: for one batch all the components were blended and then granulated and for the second batch, two excipients were added after granulation of the previously blend. Also, univariate and multivariate analysis methods were tested and compared [56].

Confocal Raman microscopy was also applied to characterize the spatial distribution of compounds in other final products such as extrudates. Kann *et al.* evaluated the spatial component distribution of a two-component formulation produced by hot melt extrusion at the surface and at one cross-section of the extrudate with CRM [45]. Qian *et al.* has applied CRM to characterize extrudates on horizontal planes that were between 100 and 200 µm underneath the surface. In this study, Raman, in contrast to DSC or XRPD, was able to detect differences in homogeneity within the samples, which had contributed to differences during the stability tests [47].

CRM was also described as a suitable technique to follow dissolution performance. Punčochová *et al.* exhibited the potential of this technique to obtain chemical images of tablets made from two different amorphous solid dispersions during dissolution both at surface and at a depth of around 20 µm [8].

Considering the previous literature, Confocal Raman microscopy has been described to have a wide range of applications. The most described application is the characterization of spatial component distribution to assess the interactions of compounds within formulations. However, CRM has also been used to investigate problems that occurred during stability test. These problems impacted the performance of the final product, due to heterogeneity within the samples [47].

The present study aims at characterizing spatial component distribution of tablets made from ASDs produced with different sieving and blending process parameters using confocal Raman microscopy.

1.7 Spectral Analysis

Confocal Raman Microscopy is an imaging technique since it provides chemical maps of the sample. Thus, a Raman spectrum is obtained for each point of the analyzed area. These spectra have to be compared to evaluate differences between the spatial points. So, hyperspectral data sets (i.e. data sets where spectral information is assigned to specific x, y, z coordinates) are generated. These data sets can be evaluated either by univariate or multivariate methods [34].

In order to perform univariate methods, a distinguishable and preferably strong band representative of the component to be studied is required [34]. Examples of univariate methods are single band intensity, bandwidth or integral. This approach is the most commonly used since it is the simplest and most directly method to produce images with chemical information about one compound within the mixture [46]. Additionally, three important considerations must be taken when using univariate methods. One is that the chosen vibrational band cannot be overlapped by the other compounds within the formulation [56]. The second one is that the studied compound cannot be present at a low concentration [46]. Finally, it is necessary to assure that the resultant image has not the contribution of unrelated intensities provided by sample focus or roughness [34]. The last condition can be satisfied by the normalization by the spectrum baseline, since the

focus affects all wavenumber of the spectrum in the same way (i.e. multiplicative factor), as mentioned in sub-chapter 1.4.1.

Bivariate analysis is simple as well and are commonly applied using ratios of two components within the sample. This method can provide also the normalization step, since the unrelated intensities do not has an impact in the relative intensities [34].

Scilab is a suitable numerical software to perform both univariate and bivariate analysis, with simple scripts that can be developed and applied for all formulations, whenever a selective band of the compound to be studied is found. In the present work, post-processing scripts were developed and implemented to perform univariate methods.

1.8 Main Objectives and Dissertation Summary

This work aims at exploring two applications of Raman spectroscopy in the development and manufacturing of pharmaceutical tablets made from amorphous solid dispersions (ASDs), in terms of both physical and chemical properties. Hence, this work is divided in two major areas of study. The first one has the aim of studying the potentialities of Raman spectroscopy as process analytical technology to predict and measure the tablets' crushing strength with a possible application to continuous manufacturing. The second one aims to evaluate the ability of Raman microscopy as an advanced characterization technique to assess the API spatial distribution on tablets produced from ASDs with different process parameters: sieving mesh size and blending shear rate. For the second study, post-processing scripts were implemented both to obtain the variation of API percentage for each tablet and to correct the focus problems.

This dissertation is divided in five main chapters:

Chapter 1 presents an introduction about Raman spectroscopy and microscopy, previous works developed in the field of Raman spectroscopy and microscopy applied in the pharmaceutical industry.

Chapter 2 is the description of materials and methods used to perform the results obtained in this work.

Chapter 3 exhibits the results obtained during this investigation and its discussion compared with previous work presented in literature whenever possible. This chapter shows the results, of the two case-studies: 1) Hardness Characterization by Raman imaging and 2) Spatial component distribution by confocal Raman microscopy and the impact of heterogeneity at a micro-scale in the performance of the final product.

In chapter 4 the conclusions of this work and the possible development in future work are presented.

The appendix presents the amorphous solid dispersion characterization.

2

Materials and Methods

2.1 Materials

Itraconazole was supplied by Capot Chemical Co., Ltd., China. The polymer hydroxypropyl methylcellulose Acetate Succinate (HPMCAS) used to produce the ASD was AQOAT® grade MG (Shin-Etsu Chemical Co., Ltd., Japan). The excipients used in formulation were hydroxypropyl methylcellulose (HPMC) (Methocel® E5, Dow Chemical, Europe), monohydrated lactose (Tablettose® 80, MEGGLE Group Wasserburg, Germany), fumed silica (Cab-O-Sil®, Cabot Corporation, USA), croscarmellose sodium (Ac-Di-Sol®, IMCD, Portugal) and magnesium stearate (Merck, Germany).

2.2 SDD Preparation

A SDD was produced, following a procedure that had already been done in the past with some modifications [57]. The formulation was produced at 40 wt.% Itraconazole load with HPMCAS MG. A solution of ITZ and HPMCAS MG was prepared with 10 wt.% solids concentration in a mixture of dichloromethane (DCM) and methanol (MeOH) (80:20). For this experiment, a BUCHI Mini Spray Dryer B-290 was used and the conditions of spray drying are described next.

A two-fluid nozzle with 0.7 mm orifice and 1.5 mm cap was used and the spray drying was performed in closed loop with nitrogen as drying gas. The flow rate of atomization was set to 0.76 Kg/h, to obtain an atomization of 38 mm. Spray dryer was stabilized with nitrogen and then with the solvent mixture of DCM and MeOH, without solids to ensure a stable inlet and outlet temperature. The outlet temperature (T_{out}) was set to 40 ± 1 ºC to guarantee an effective drying. To achieve the T_{out}, the inlet temperature (T_{in}) must be set around 62ºC and the condenser temperature (T_{cond}) -5 ºC. The feed flow rate was set to 32% in the peristaltic pump, which is equivalent to 11.5 mL/min approximately. The dried powder was collected with a high-performance cyclone.

In order to remove any residual solvents, a post-drying step was performed in a vacuum drying oven Vaciotem-TV (JP Selecta, SA., Barcelona). The operation occurred at a temperature of 40 ºC, under vacuum at approximately 0.2 bar, and with nitrogen sweep, for approximately 8 hours. After that, a thermogravimetric analysis (TGA) was performed to ensure the effective drying of the powder.

2.3 Blend and Tablet Preparation

In Table 2.1, the formulations used in this work are presented.

Table 2.1 - Formulations

Components % (w/w)	Formulation I	Formulation II
Spray Dried Dispersion	60.00	56.84
HPMC	20.00	18.95
Monohydrated Lactose	13.50	12.79
Fumed Silica	1.00	0.95
Croscarmellose Sodium	5.00	10.00
Magnesium Stearate	0.50	0.47
Drug load (%)	24.00	22.74

The aim of this work is to analyze tablets with different process parameters, following two designs of experiments (DoE). The blend preparation was different for each design and the procedure is explained for all the designs.

2.3.1 DoE I - Hardness Characterization

In order to understand tablets hardness and its influence in the Raman spectra baseline, different compaction forces were applied to produce the final dosage forms (all other blend process parameters were maintained constant). The formulation used to perform this mixture was formulation I, described in Table 2.1. The SDD was sieved through a sieve with apertures of 850 µm and the excipients were sieved through a mesh size of 800 µm. The mixture was performed in a TURBULA® T2F, System Schatz., for 2 minutes and with 46 rotations per minute (rpm). After that, the magnesium stearate was added, and the mixture was blended again, this time for 1 minute with 22 rpm.

Round and flat faced tablets were produced with a diameter of 12 mm with a PMS M press ST-8. The weight of the tablets was 400 mg. The physical mixture was compressed to obtain seven different crushing strengths: 10, 40, 70, 105, 135, 170 and 190 N.

2.3.2 DoE II - Spatial Component Distribution

For this study, five different experiments were produced with different process parameters: sieving and blending. The mesh size used in the SDD sieving was varied in two levels. The blending shear rate of the mixture, before adding the magnesium stearate, was also varied in two levels. The blending shear rate was defined as the rotation speed, maintaining 100 rotations in total. A central point of the two parameters was studied as well.

These parameters were varied between 600 and 2000 µm mesh size and 22 and 96 rpm. The central point tested was prepared at 46 rpm and the mesh size was 1000 µm (Figure 2.1). In all the experiments of this design, formulation II was used, and all the excipients were sieved through a mesh size of 800 µm. The mixture obtained after adding the magnesium stearate was blended for 1 minute at 22 rpm, in all experiments.

Round and flat faced tablets with 340 mg and a diameter of 10 mm were compressed using a PMS M press ST-8 to obtain a crushing strength of 80 N.

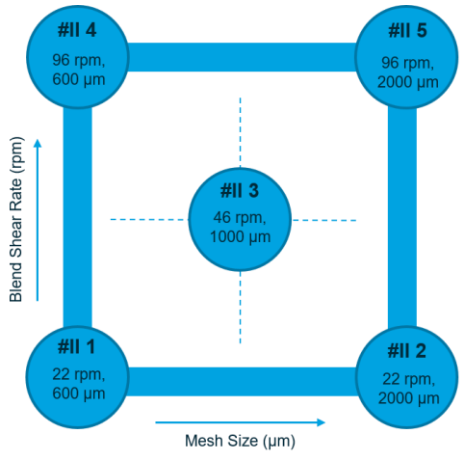

Figure 2.1 - Design of Experiments for Heterogeneity Studies

2.4 SDD Analytical Characterization

Thermogravimetric analysis (TGA)

To guarantee the effectiveness of the post-drying step, a TGA was executed in a TGA 550 from TA Instruments (USA). Two samples were tested, since the post-drying step occurs in two different trays. The samples weighted 21.0712 and 21.9662 mg and were heated at 10ºC/min rate until reach 350ºC.

Differential Scanning Calorimetry (DSC)

To determine the glass transition temperature of the sample of the SDD, a modulate DSC (mDSC) analysis was performed in DSC 250 (TA Instruments, USA). The sample with 5.653 mg, placed in a pinhole hermetic pan, was equilibrated at 25ºC. The purge gas was nitrogen and the

flow rate was set to 50 mL/min. Afterwards, a modulated heating ramp was performed to 350ºC, at a heating rate of 3ºC/min, using an amplitude of 0.48ºC at every 60 seconds.

Particle Size Distribution

The particle size of spray dried dispersion of ITZ was analyzed by laser diffraction in a SYMPATEC, Sympatec Inc., USA, following the USP requirements [58]. The dried powder was sampled in a proper vial for the purpose. Then, the dispensing unit RODOS/M applied a pressure of 3 bar at a feed velocity of 18 mm/s and a laser diffraction sensor HELOS measured the sample within a range of 0.5 µm to 350 µm.

X-Ray Powder Diffraction (XRPD)

In order to assure that SDD was in amorphous form, a XRPD analysis was performed, mimicking a previous work, with an Empyrean Alpha 1 X-ray diffraction system (Malvern PANalytical, Netherlands) with Reflection Transmission Spinner configuration. A ceramic diffraction X-ray tube made of anode material, Cu (λ = 1.54 Å) was used and operated at a voltage of 45 kV and a current of 40 mA. The scan range was set between 3.00 and 40.00º. The sample was analyzed with a step size of 0.0167º at a time per step of 59.690 seconds. The total time of data acquisition was 18 minutes, approximately.

2.5 Final Dosage Form Characterization by Raman Imaging

For all the experiments presented in this master thesis, a Confocal Raman Microscope Alpha 300 RA, from WITec equipped with a laser of 532 nm wavelength was used. The laser power was set to 10 mW and the integration time was 1 second, for all the experiments.

2.5.1 Choice of General Analysis Parameters

With the aim of assuring quality in Raman spectroscopy, the parameters to perform the analysis were chosen carefully. The signal-to-noise ratio(SNR) was assessed, since it measures directly the quality of the resultant spectra data [33], [59]. A *Scilab* script was developed to determine the SNR of all the samples studied. To determine the SNR of spectra data, both test and blank samples were considered. The noise was determined by the standard deviation of the blank measurements. The signal is the difference between the intensity of the test sample and the intensity of the blank sample for the peak of interest [59], [60].

Laser Power

As mentioned before in sub-chapter 1.4.1, laser power is an important parameter to be defined. Thus, in this work, three laser powers were studied: 10, 15 and 20 mW and the resultant fluorescence were compared between these experiments. Fluorescence background is a major problem when performing Raman spectroscopy, due to the low cross section of Raman scattering. Relative to the Raman signal the fluorescence background can be up to 10^8 times stronger

[34]. By fitting a polynomial of an order high enough to describe the slow varying fluorescence spectra, but not the sharp Raman peaks. Subtracting this polynomial from the spectra will remove or at least reduce the influence of fluorescence and yield only the Raman peaks. A first order polynomial function was thus fitted to all spectra data and the fluorescence was measured as the slope of the fitting curve. As can be seen in Figure 2.2, the fluorescence can be reduced with the reduction of the laser power.

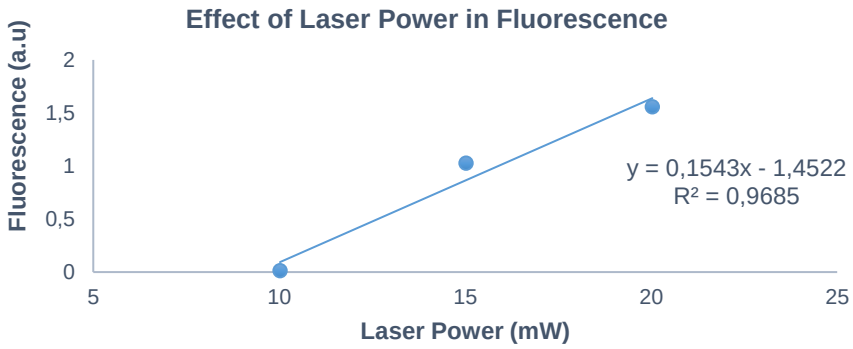

Figure 2.2 - Effect of Laser Power in Fluorescence

Since raw data is going to be directly used to obtain the results, it is imperative to choose a laser power to minimize fluorescence and, on other hand, maximize the SNR. Consequently, 10 mW was the value of laser power chosen to this method development and all the experiments were done maintaining this parameter constant.

Temporal Resolution

To study the impact of acquisition time in the resultant spectra, the SNR was studied for the same position in a sample, using as acquisition times 0.5, 0.8 and 1.5 seconds, maintaining the number of acquisitions constant. Complementarily, the influence of number of acquired spectra was evaluated, testing 10, 20 and 50 acquisitions for each acquisition time. Figure 2.3 and Figure 2.4 show this influence, respectively. A trend line was then determined for each experiment. The figures show the SNR as function of acquisition time and as function of the number of accumulations. The slope of the trend lines can give an information about the influence of these parameters. The acquisition time is the parameter that has the greatest influence in the quality of the signal [33] and this can be verified by the higher slope of the trend line, compared to the trend line of Figure 2.4.

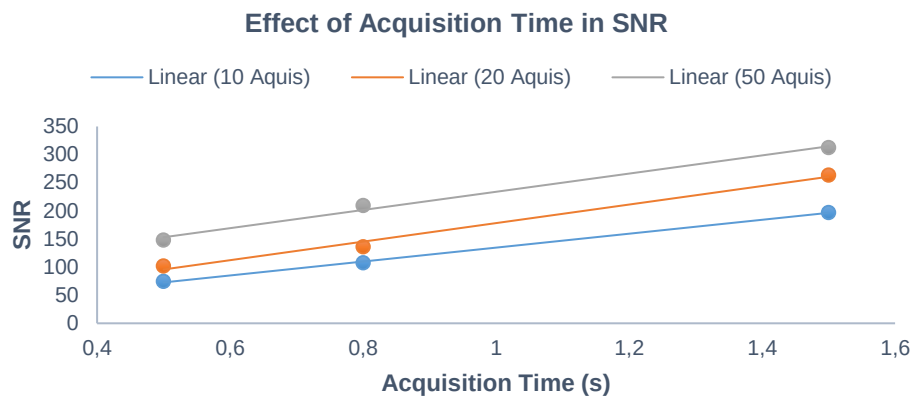

Figure 2.3 - SNR as function of acquisition time

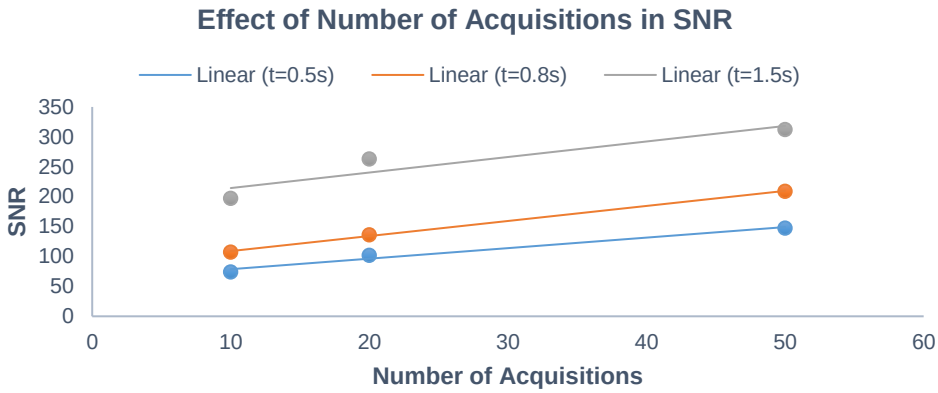

Figure 2.4 - Variation of SNR as function of number of acquisitions

Other way to notice this difference between the impacts of these two parameters is to represent the SNR as function of total acquisition time, calculated as the acquisition time multiplied by the number of acquired spectra. As can be seen in Figure 2.5, the SNR obtained with 10 spectra of 1.5 seconds each is higher than for the SNR obtained with 20 spectra of 0.8 seconds each.

For the present work, the integration time was set as 1 second, considering the SNR obtained and the time to perform all type of analysis: single point and large area scan. The number of accumulations was set as 10 for single point analysis.

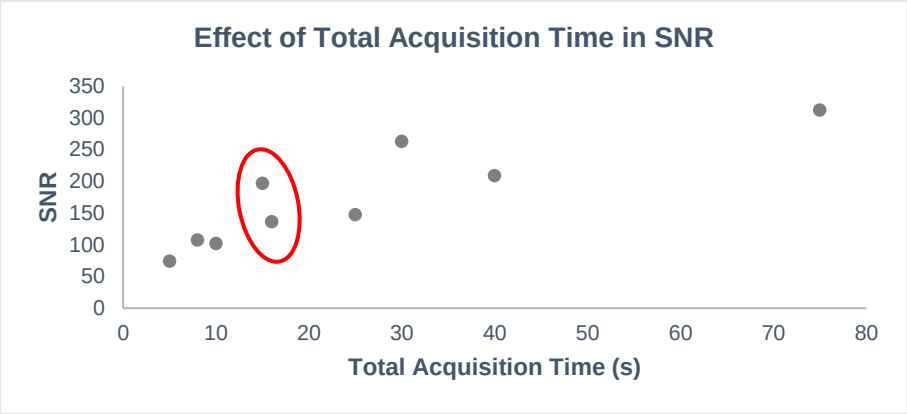

Figure 2.5 - Effect of Total Acquisition Time in Signal Quality

Focus Plane

In this work, a confocal Raman microscope was used as an imaging technique and as previously mentioned in sub-chapter 1.4.1, the signal will be properly yield only in focused samples. Figure 2.6 shows how the same sample in-focus and out-of-focus has different relative intensities of Raman peaks. As can be seen in Figure 2.6, the quotient between the signal of sample in-focus and out-of-focus is a constant function and thus the difference between the two signals is explained by a multiplicative factor [34].

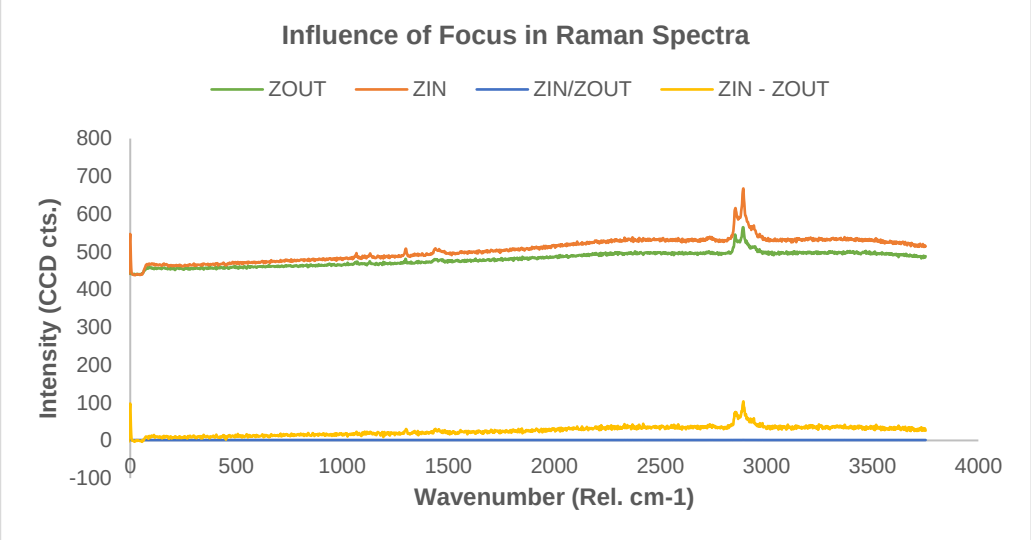

Figure 2.6 - Influence of focus in Raman spectra (sample in-focus: orange; sample out-of-focus: green; signal subtraction: yellow; quotient between the signals: blue)

Since the focus plane is an important parameter to be considered [33], the tablets used in this study were produced to have a flatted surface. However, they are composed by porous materials, which cause some roughness. So, the ideal focus plane was not at the surface, but beneath the surface to overpass the top rough surface, as described already in the literature [30]. The apparatus enables analyses beneath the surface up to -100 µm Z plan. The analyses were

performed at surface and beneath the surface at -20 µm Z plan since the tablets were made of opaque material.

In summary, the analysis type is always set according to the material under study. For the first case-study, single point analysis was performed. On the other hand, for the second case-study, large area scan analyses were performed, with different spatial resolutions and different depth focal planes.

In this master thesis, all data was processed by univariate methods with *Scilab* scripts, developed during the study.

2.5.2 Hardness Characterization

To explore the Raman potentialities as a PAT to measure the hardness of tablets, tablets of seven different crushing strengths were analyzed to understand if there was a feasible correlation between the spectra baseline and the tablets crushing strength. Similar studies using Raman spectroscopy were already described in chapter 1.5.

For each crushing strength, three different tablets were analyzed with single point mode in CRM to better simulate the analyses in continuous manufacturing. Each tablet was analyzed in five equidistant points (Figure 2.7) and the result was one single spectrum for each point, obtained with 10x objective lens, at a laser power of 10.0 mW. The spectra were obtained with an integration time of 1 s and 10 accumulations per point.

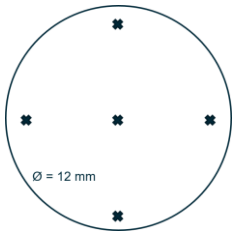

Figure 2.7 - Representation of Raman Analysis in five points

Afterwards, an average of the five points was performed and one spectrum was obtained for each tablet. A software for numerical computation, Scilab, was used to analyze the Raman spectra. A Scilab script was developed to determine the area under the spectra in four different bands, represented with orange color in Figure 2.8.

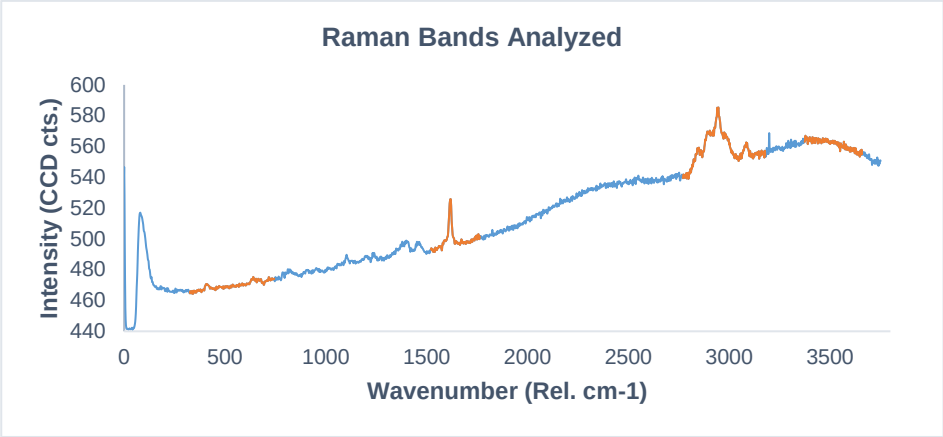

Figure 2.8 - Analyzed bands in the Raman spectrum

The spectral bands between wavenumber 326 and 744 (rel. cm^{-1}), and 3374 and 3658 (rel. cm^{-1}) represent only the baseline of the spectrum since no peaks appear in these bands. The two bands were analyzed to understand if the fluorescence effect was impacting on the baseline differences. The spectral band between wavenumber 1516 and 1759 (rel. cm^{-1}) is the selective API peak correspondent band and the spectral band between 2771 and 3179 (rel. cm^{-1}) corresponds to HPMC AS: the polymer used to produce the amorphous solid dispersion.

The areas of the spectral bands were compared for both the seven different experiments and the three tablets within the same experiment to evaluate the variability between and within the experiments, respectively. Then, the average of each spectral band area for each experiment was plotted as function of the crushing strength to determine if there was a correlation between these two parameters.

2.5.3 Spatial Component Distribution

This work aims at exploring the potentialities of Raman microscopy as an advanced characterization technique to evaluate the spatial component distribution within tablets.

Five different experiments were produced with different process parameters: sieving and blending. Each tablet was analyzed with Raman in three adjacent areas with the same size (6000 x 2000 µm) and same spatial resolution (50 µm). The center of each area was: the middle of the tablet (0, 0) µm, the top of the tablet (0, 2000) µm and the bottom (0, -2000) µm. These areas cover ca. 46 % of the tablet area and are represented in Figure 2.9. Raman analyses with these conditions were performed in triplicate for each experiment and the total time of analysis for one tablet is 4 hours. Then, to obtain a more resolved image, a Raman analysis was performed in the center of the tablet with a smaller size (1000 x 1000 µm), and greater spatial resolution (5 µm). Since this analysis takes 11 hours to be executed, just one tablet was evaluated in these conditions, for each experiment.

Spectra were obtained with the 10x objective lens, a laser power of 10.0 mW and an integration time of 1s, for the both spatial resolutions analyses.

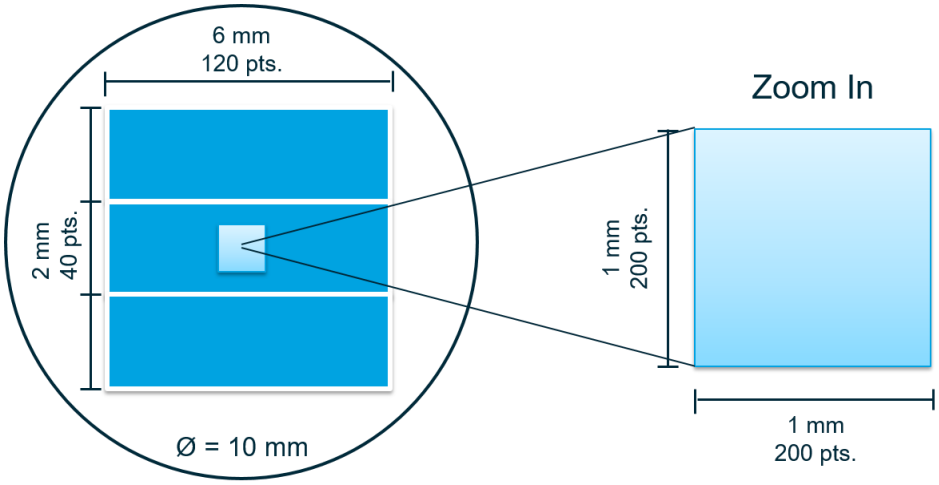

Figure 2.9 - Representation of Raman Analysis (50 µm and 5 µm of spatial resolution)

Additional analyses were performed to understand the API distribution beneath the surface of the tablets, which is the ideal focus plane, as previously mentioned. Spectra were obtained with the same conditions as for the greater resolution area, but in a Z plane of -20 µm. For each experiment, only one tablet was evaluated under these conditions, given the necessary time to perform an analysis (11 hours).

CRM provides a spectrum for each point within an analyzed image. To easily interpret the spectral information given by the apparatus, a Scilab script was implemented to evaluate the spatial API distribution within the image.

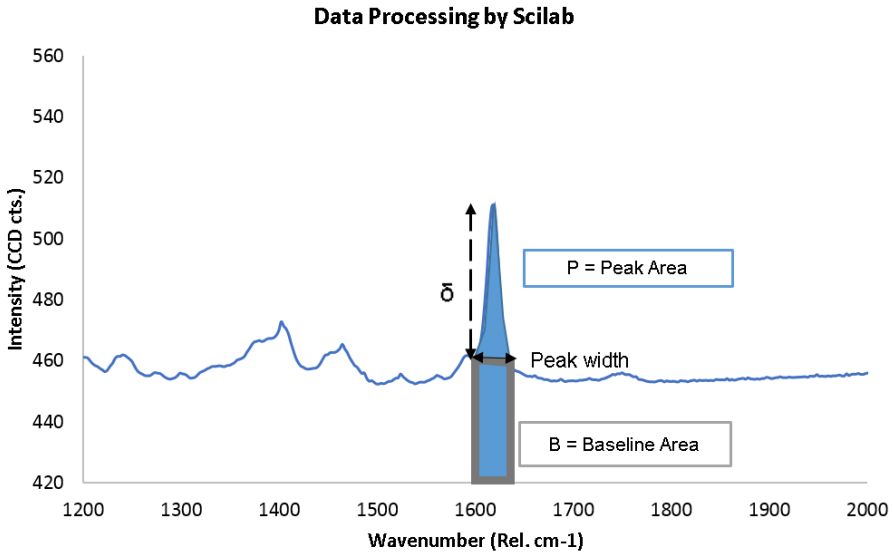

Figure 2.10 - Schematic Representation of Data Processing by Scilab

Following the schematic representation in Figure 2.10, delta (δ) represents the subtraction between the total area of a selective API peak (i.e. Peak Area (P)) and the baseline area (B) within the same integration limit. With the aim of correcting focus problems, δ was divided by the baseline area (B) and a δ/B was obtained for each point within the image. Next, this calculation was performed also for the Raman spectrum of the pure compound and a δ/B of the pure compound (δ/B_{PURE}) was obtained. Afterwards, the δ/B of each point within the image was compared to the δ/B_{PURE}, to determine the API percentage of each spatial point of the image. The baseline is used as the reference for the focus plane, since the sample in-focus and out-of-focus have different relative intensities of Raman as explained in chapter 2.5.

After this normalization, the average of API percentage in the image was determined. The averaged percentage was subtracted from the API percentage in each point to represent the variation of API percentage relative to the average. The variation of API percentage is presented as a variation of color in the chemical maps of the tablets.

2.6 Hardness Analysis

The hardness of the tablets was measured as crushing strength tested in a Manual Tablet Hardness Tester HT1 (SOTAX AG, Switzerland).

2.7 Disintegration Analysis

The disintegration was performed in a Disintegration Tester ZT 320 Series (ERWEKA, Germany), following the US Pharmacopeia (USP) [61]. The tablets were placed in the tubes of the basket and a disk was added. The apparatus operated using a solution of HCl (0.1 N) as the immersion fluid, maintaining its temperature at 37 ± 1°.

3

Results and Discussion

The present work has the aim of linking process, product and performance, with Confocal Raman Microscopy, since critical process and formulation factors can greatly impact the quality and performance of pharmaceutical final products [5].

This study is divided in two major areas: 1) hardness characterization and 2) spatial component distribution. In the first one, compaction force was varied to obtain a range of tablet's crushing strength and to evaluate the impact on the Raman signal obtained. The aim of this case-study was to understand if a feasible correlation exists between tablets' hardness and Raman spectra. For the second study, a DoE was defined where sieving mesh size and blending shear rate were varied aiming to obtain differences in API distribution within the tablet which were quantified with Raman imaging. The impact of heterogeneity at a micro-scale on the performance of the final drug product was also assessed. The results of each case-study are shown and discussed in this chapter.

3.1 Hardness Characterization

In a continuous process, tablets are produced on a high-speed rotary tablet press [62] continuously fed by in-line blenders which mix API or spray dried material with tableting excipients enabling a large throughput and a variable production volume [15]. However, tablets quality control often requires destructive methods such as diametral compression test, disintegration and/or dissolution [15], [23], [54] , which are performed on periodic time-points or at the end of the production. This can lead to production challenges when a process deviation occurs which is only detected later during Quality Control and can jeopardize the entire production since the last Quality Control time point, leading to production delays and material costs.

To overcome these challenges, spectroscopy techniques have been proposed as process analytical technologies to predict tablets' physical properties such as mechanical strength (hardness), friability, porosity and density which enable in-built quality control and real time release [5], [15], [22]–[24]. Furthermore, Raman spectroscopy has the advantage of being highly sensitive to

changes in the molecular structure and thus the spectra are influenced by both chemical and physical factors [55].

The aim of this study is to investigate whether the tablets' mechanical strength can be reliably measured by Raman spectroscopy for tablets containing amorphous solid dispersions as has been previously suggested for tablets containing of crystalline API [23], [24], [55]. As a case-study, the manufactured ITZ:HPMCAS SDD (sub-chapter 2.2), was used to manufacture tablets with seven different crushing strengths from 10 to 190 N by varying the compression force. Although a Raman probe, rather than a confocal Raman microscope, would be more appropriate for such a measurement, since it would typically measure the spectra of the whole tablet surface [64], tablets were evaluated in five points. To study the influence of the tablets' crushing strength in the baseline of the Raman spectra, an average of the spectra of these five points was done, for each tablet. Then, an averaged spectrum was obtained with the previously explained conditions (sub-chapter 2.5.2) for each experiment (triplicate trials). The averaged spectrum of the first tablet of each experiment is presented in Figure 3.1. The response within a spectral band selective of the API peak is shown in Figure 3.2.

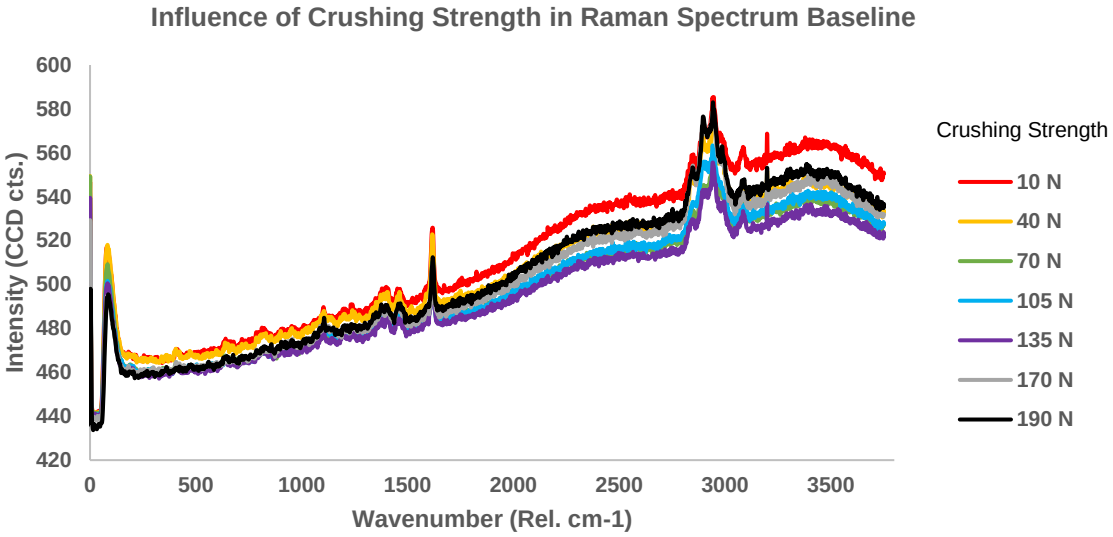

Figure 3.1 - Influence of Crushing Strength in Raman Spectrum Baseline

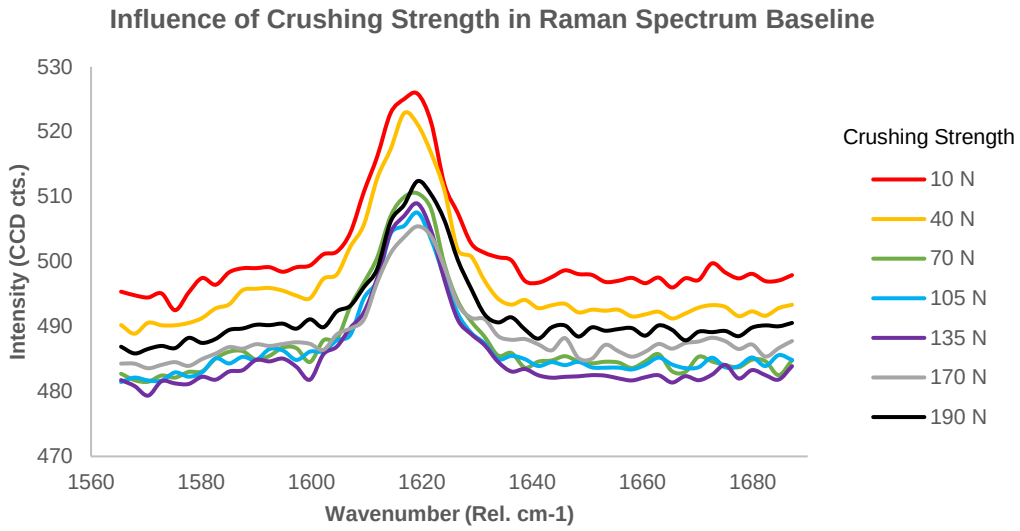

Figure 3.2 - Influence of Crushing Strength in Raman Spectrum Baseline: selective API peak area.

The data do appear to confirm that there is an impact of the tablets' hardness on the Raman spectra baseline for the amorphous-based tablets similarly to what was reported in the literature for crystalline-based tablets. However, the impact on the spectra appears to have two regimes: from 10N to 40N the baseline decreases, but from 135 N to 170N the baseline increases. Remarkably, even for crystalline-based tablets both behaviors have been reported. On the one hand Wang *et al*. and Heigl *et al*. [24], [55], reported a baseline decrease with the hardness, but on the other hand Virtanen *et al*. [23] reported baseline increase with the hardness. Noticeably, in the literature the authors have focused on the qualitative response rather than presenting quantitative data which is necessary to understand if there is a feasible correlation between Raman spectrum baseline and the tablets' crushing strength. The area under the analyzed bands was determined and the crushing strength was evaluated by the diametral compression test, for each tablet. Figure 3.3 presents the area under the band between 3374 and 3658 (rel. cm^{-1}) as function of the crushing strength determined by the destructive test.

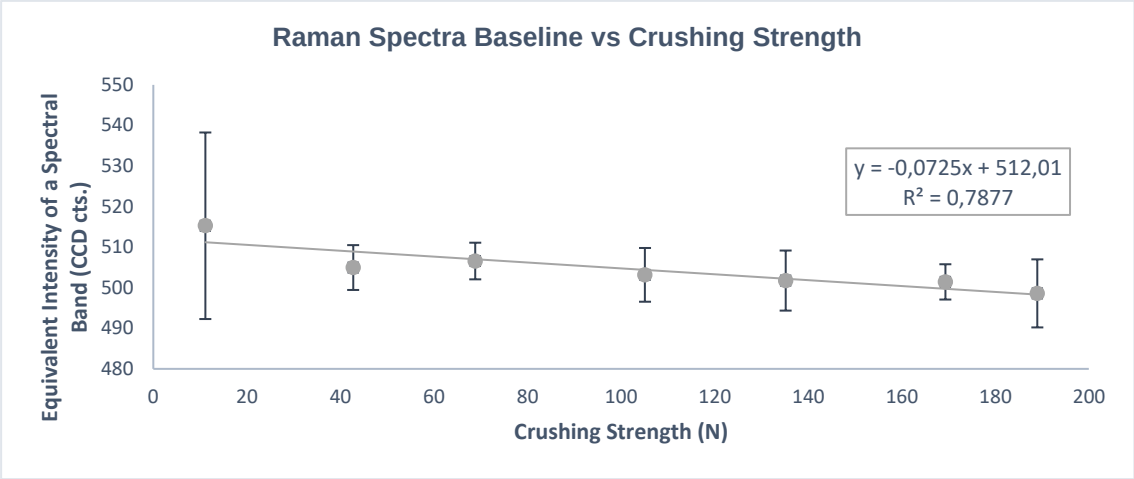

Figure 3.3 - Influence of Crushing Strength in a Spectral Band Area

The equivalent intensity of the spectral band varies between 500 and 520 (CCD cts.). The average area of the spectral band is not strictly monotonic with the crushing strength and the variability of the Raman imaging analysis is comparable to the change in average spectral area for the measured crushing strength range. This variability is much greater for the experiment of lower crushing strength possibly due to the higher roughness of the tablets of this experiment, when compared to the higher levels of crushing strength. The variability between all the experiments can also be explained by sub-sampling, since in this study just five points were analyzed. A larger surface area of the tablet should had been analyzed, which would substantially lower the assessment error, as previously described by Johansson *et al*. [22].

The influence of tablets' hardness in Raman signal was reported to depend on the setup used and formulation studied, given that spectroscopic techniques can yield different results due to spatial variations and inhomogeneities of the sample [22], [23]. Hence, a possible explanation of the results can be the formulation used in this study, since tablets composed of amorphous solid dispersions were analyzed. As far as the literature is concerned, no author has reported the influence of tablets' hardness in Raman signal, for tablets produced from ASDs.

In this work, a confocal Raman microscope was used. As explained in chapter 1.4, with this technique the scattered light from different spots not included in the focal plane does not contribute to the produced image [29], [33], [39]. If a large area of the tablet had been analyzed, Raman signal could possibly be influenced by variations in surface roughness. An increase in tableting compaction force increases the tablets' hardness [63] and reduces the tablets' surface roughness [64]. Thus, surface roughness would probably be a good parameter to indirectly infer tablets' hardness [23].

Even though the methodology studied did not result in a predictive model for tablets' hardness characterization, CRM was proved to evaluate the stability during processing of the amorphous solid dispersion within this design space. The ASD analytical characterization provided by complementary analytical methods is described in Appendix A. For this formulation, the API maintained its amorphous form in the range of compaction forces studied (Figure 3.4), as previously described for other formulation during the tablet manufacturing for a wide range of compression forces [18]. By the previous literature, it is known that ITZ amorphous content within tablets has been also assessed by Raman spectroscopy [49] and the conversion of polymorphs forms has already been described using micro-Raman spectroscopy [66].

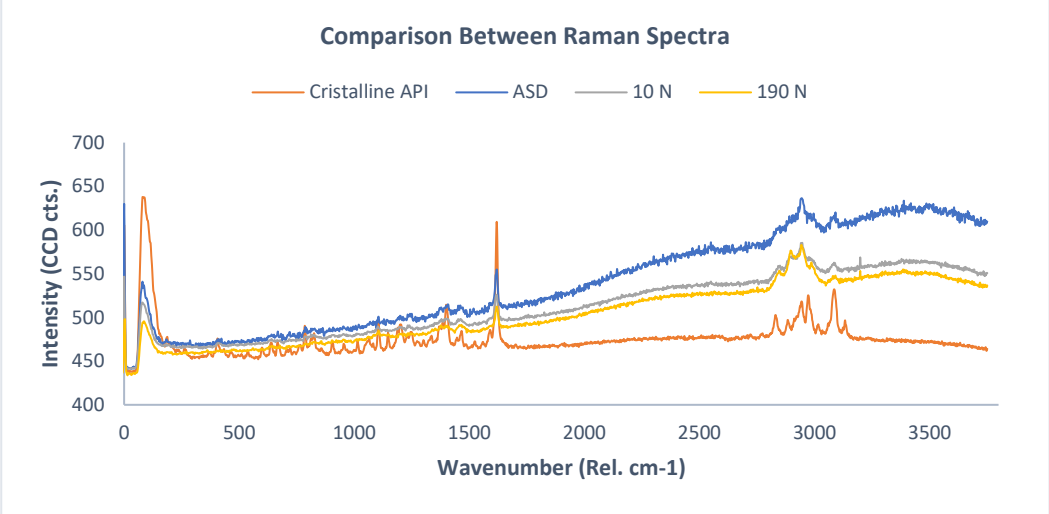

Figure 3.4 - Comparison between Raman spectra: crystalline API (orange), ASD (blue), Crushing Strength of 10 N (grey) and Crushing Strength of 190 N (yellow).

In conclusion, a predictive model of Raman spectroscopy to measure tablet's crushing strength was not achieved. However, these results were obtained for a single pharmaceutical formulation and using solely a confocal Raman microscope which has a narrow field of view. This has the disadvantage of requiring a large number of single point measurements for the average to be representative of the spectrum of the entire surface of the tablet. Nevertheless, the observations that (i) the average change in the Raman spectra baseline is small even for an order of magnitude change in mechanical strength and (ii) that the relation between the two is not monotonic may carry over for whole surface measurements.

3.2 Impact of Sieving and Blending on the Spatial Component Distribution

During formulation development, it is important to investigate the interactions between the API and the excipients within the range of formulations studied, as well as their distribution within a tablet. To test these parameters, formulations are tested in terms of blend homogeneity by bulk uniformity analysis [65] and after tableting, the final drug product is tested by content uniformity

[66] to assess on heterogeneity between tablets from the same batch [66]. Tablets are also tested in terms of performance by disintegration [61] and dissolution tests [28].

These techniques can only assess heterogeneity at a macro-scale since the response of bulk uniformity analysis is based on different resultant API concentration in different points of the mixture [62]. Content uniformity analysis is based on the comparison of the assay of individual tablets of the same batch. Thus, this technique cannot assess on the agglomeration of compounds when the assay is constant for all tablets of the same batch. On the other hand, the heterogeneity at a micro-scale was shown to impact the performance of the final products [47]. So, it is necessary to evaluate the heterogeneity at a micro-scale by characterizing the spatial components distribution within the final product. Confocal Raman microscopy is a suitable technique for this evaluation, given that it can provide spatially highly-resolved chemical maps [9]. CRM has been described as an adequate tool to provide information on homogeneity of tablets and the distribution of ingredients within a formulation down to the inter-particle mixing [33].

This study aims to evaluate the API spatial distribution using CRM. For that, a structured 2-level design of experiments with an additional central point was performed, giving a total of five experiments. Two important process parameters that impact in the homogeneity of the final product were varied. The first parameter was the sieving mesh size during sieving step which is known to break-down agglomerates [67]. The second one was the blending shear rate. The shear rate is measured as the velocity at which layers move past each other [68]. In this study, blending shear rate was varied as the rotation speed to perform the mixing using for all the experiments flasks with the same volume. The number of vessel rotations was kept constant for all the experiments.

The five experiments were evaluated by CRM, as described in sub-chapter 2.5.3. The result of each point in the spatial dimension is a Raman spectrum. A Scilab script was developed to interpret the variations of the spectra between the spatial coordinates and to correct focus issues. The script (explained in sub-chapter 2.5.3) was developed to determine the variation of the API selective peak, within the analyzed spatial area. The variation of API was normalized by the average of API percentage.

The result is a two-dimensional image of the tablet, where the API variation is represented by color variation. In the color bar, the green color represents no variation of API relative to the average. The maximum value is represented as red and the minimum value corresponds to blue. The first one corresponds to 25 percent above the average and the second corresponds to 25 percent below the average.

First, the results for the tablets analyzed by large area scan with 50 µm spatial resolution at the surface are presented for the five experiments in triplicate. The image size is 6000 x 6000 µm, as it represents the three adjacent areas evaluated for each tablet (see Fig 2.9 for detailed explanation). Each point within the image represents 50 µm.

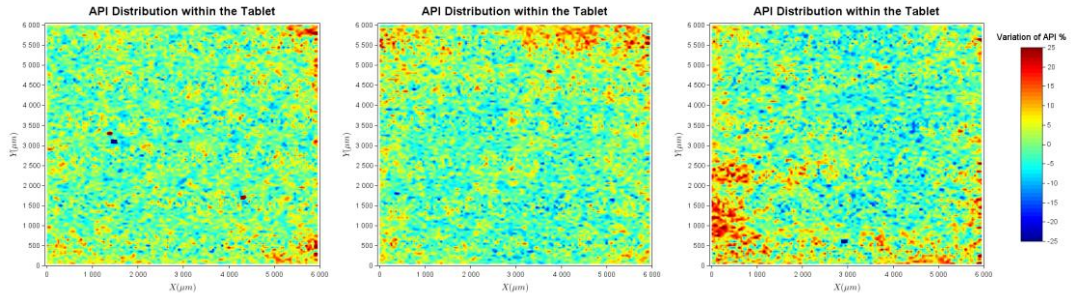

Figure 3.5 - API distribution within the tablet (50 µm spatial resolution): experiment three independent tablet analysis

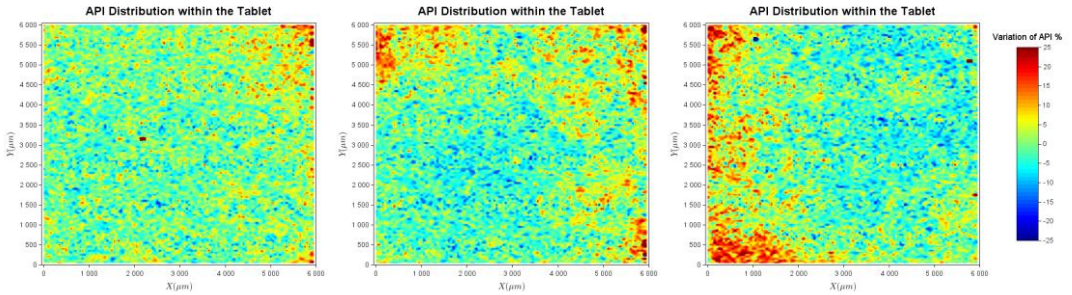

Figure 3.6 - API distribution within the tablet (50 µm spatial resolution): experiment 2 three independent tablet analysis

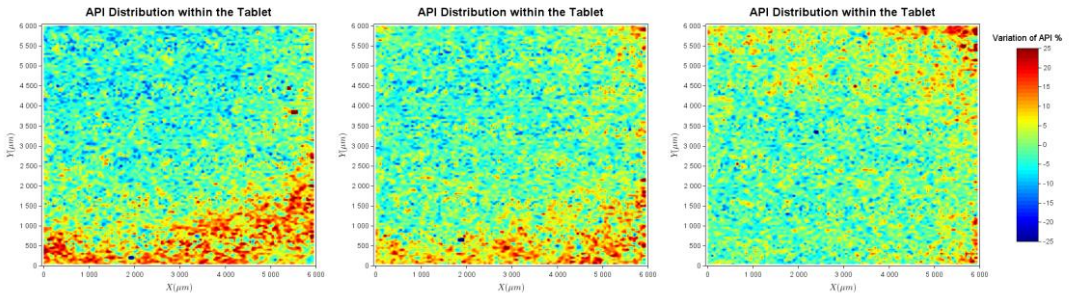

Figure 3.7 - API distribution within the tablet (50 µm spatial resolution): experiment 3 three independent tablet analysis

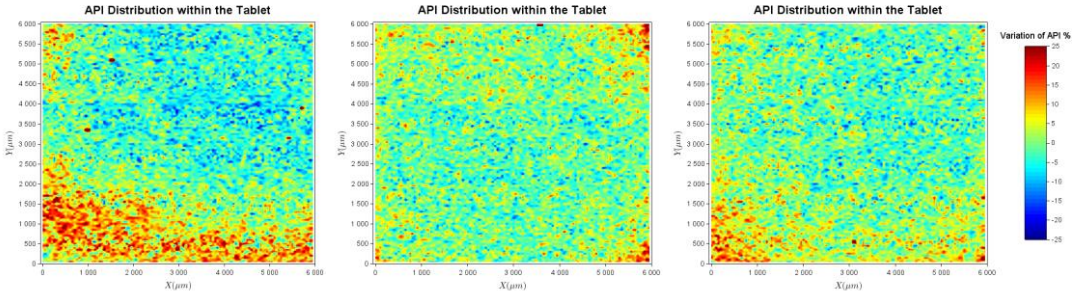

Figure 3.8 - API distribution within the tablet (50 µm spatial resolution): experiment 4 three independent tablet analysis

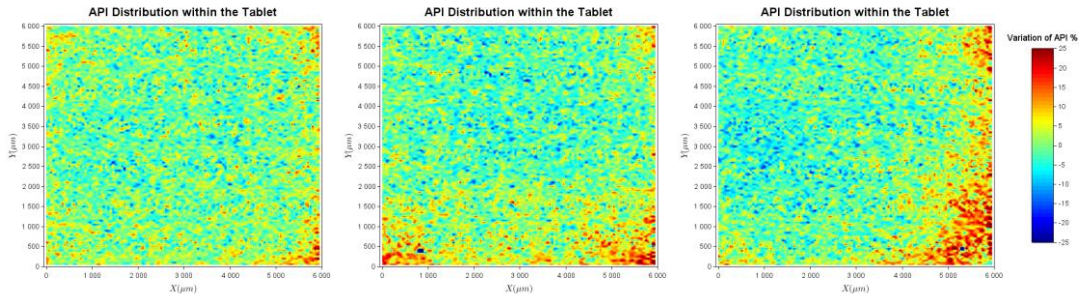

Figure 3.9 - API distribution within the tablet (50 µm spatial resolution): experiment 5 three independent tablet analysis

The above figures (Fig 3.5 to 3.9) describe the spatial distribution of API. The API seems to not be homogeneous within all the images, since in some images, an accumulation of red spots is seen (for example Fig 3.8, first image: in the lower end, a band of red spots is detected, corresponding to an accumulation of API). Interestingly, some tablets showed API accumulation near the borders of the images. Since this analysis is performed at the surface of the tablets a possible explanation for these results can be the differences between focus planes. As explained before, in this work, a confocal Raman microscope was used and with this methodology, just the points within the focal plane yield good Raman signals. It is difficult to ensure that the points within a large area of a tablet's rough surface are all in the same focal plane. A way of confirming whether this heterogeneity is due to different focus plans or, in fact, attributed to sample heterogeneity, would be to perform the analysis in a middle focus plane (i.e. a few micrometers under the surface), as already described by Helešicová *et al.* [30] or if a longitudinal section of the tablets had been evaluated.

Possible surface phenomena such as sticking (i.e. material transfer onto the surface of the tablet punch) during tableting process [69] and accumulation of powder at the surface can have been addressed by Raman. This issue could have been solved if a longitudinal section of the tablets had been evaluated. Another possible solution could be the application of a complementary technique that can address surface properties. Applying this solution would provide the characterization of the surface regarding topography and hardness. Combining these techniques with chemical information would give a full characterization of the final product. Previous authors has successfully implemented the combination of Raman microscopy with optical profilometry [45] and with atomic force microscopy (AFM) [70] to characterize different drug delivery systems.

The information provided by the chemical maps can also be presented by histograms, as described by the previous literature [19], [26]. A histogram representing a normal distribution with small standard deviation would correspond to homogeneity within the sample.

Next, the histograms corresponding to the above chemical maps are presented (Figure 3.10). The histogram represents the number of points within the image that corresponds to each

value of API percentage variation. This variation goes from 25 percent below the average of API percentage to 25 percent above the average.

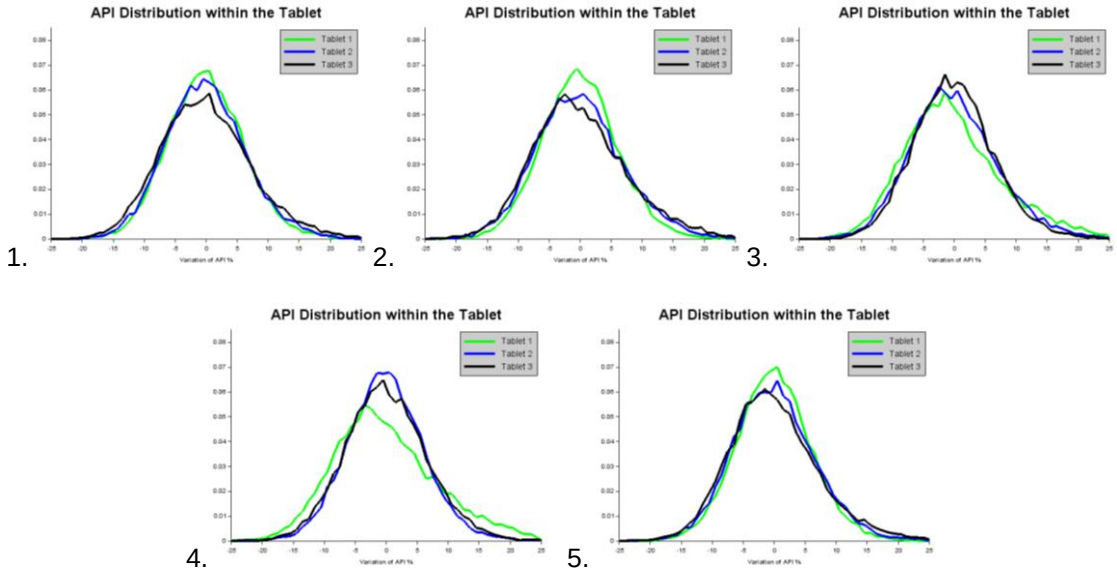

Figure 3.10 - Histograms of API distribution within the tablet (50 µm spatial resolution). The experiments 1, 2, 3, 4 and 5 are represented with the correspondent numbers.

The above histograms present a unimodal distribution, which can indicate the absence of heterogeneity at a macro-scale. In general, the histograms mode is near to zero (i.e. no variation relative to the average of API percentage). This can show that most points within the image corresponds to the average of API percentage. If the histogram's mode is located at lower or higher values of API percentage it can mean that there is absence or accumulation of API in the chemical map, respectively. These differences can happen in cases of heterogeneity at a macro-scale in which the API content of tablets varies in the same batch. Specifically, the first tablet of the fourth experiment is presented as a broad distribution. The histogram's mode is located at lower values of API percentage indicating the possible absence of API. This can be verified by the chemical map, as the most part of the image is blue colored.

In a global view, the distribution presented in histograms indicates the absence of heterogeneity at a macro-scale. There was evidence of possible heterogeneity at a micro-scale. However, the heterogeneity at this spatial resolution at the surface can be possible explained by focus issues, as explained above.

To obtain more information about heterogeneity at a micro-scale, it is important to evaluate possible agglomerates at the scale of the SDD particles. The SDD's particle size is ca. 5 µm. So, a greater spatial resolution (5 µm) was studied at the surface of the tablets and the results are presented next (Figure 3.11) for the five experiments. The color bar is the same as presented before and the variation of API percentage is between 25% less and 25% more than the average.

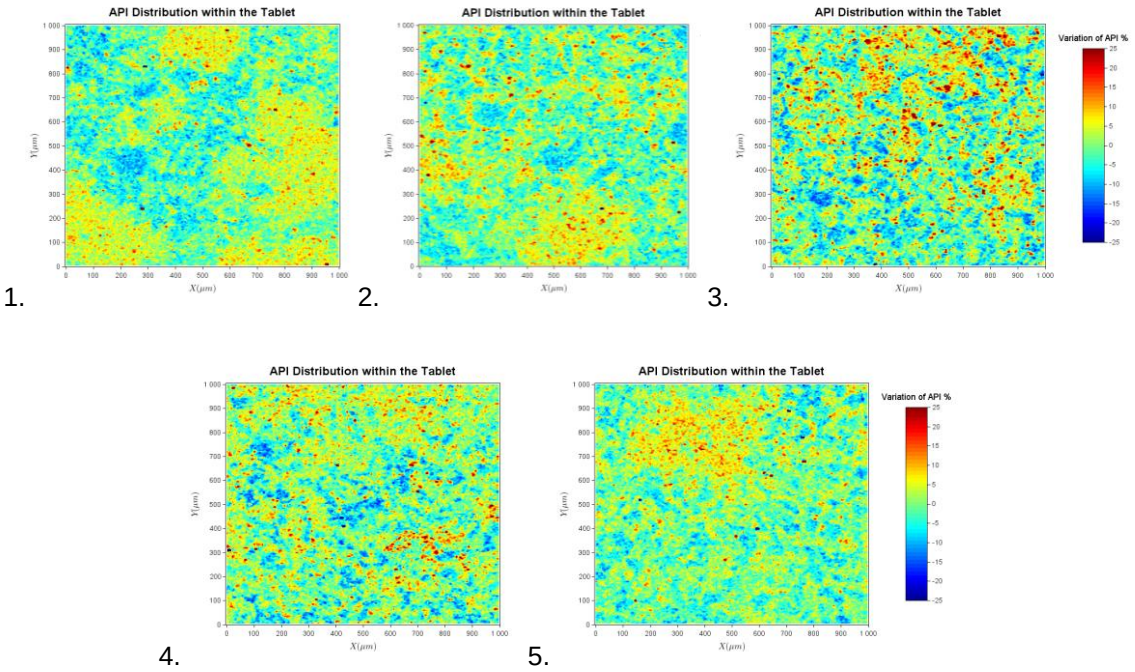

Figure 3.11 – API distribution within the tablet, evaluated with 5 µm of spatial resolution, at the surface of the tablet (Experiments 1, 2, 3, 4 and 5 are represented with the correspondent numbers)

For the images above, at the range of the SDD particle size, the accumulation zones detected previously (as accumulation of red spots) are not seen. Since each point analyzed in this area corresponds to the size of an SDD particle, a full distribution of color should be seen corresponding to the percentage of API within the tablet (~22.7%). As seen for the wider distribution (50 µm) the evidence of heterogeneity at the surface can be influenced by surface issues. A Confocal Raman Microscope was used and thus the surface of the tablet must be perfectly flat. That could not be achieved, since the tablets were made of a porous material. Therefore, Raman analyses were performed beneath the surface to ensure that the quality of the data was not influenced by different focus planes and to not assess the possible effects of the surface. So, the samples were focused at a Z plane under the surface of the tablet at -20 µm in depth. This depth was chosen considering a previous work in which good chemical images of the tablets were obtained with this methodology [8]. A spatial resolution of 5 µm was evaluated and the results are presented in Figure 3.12.

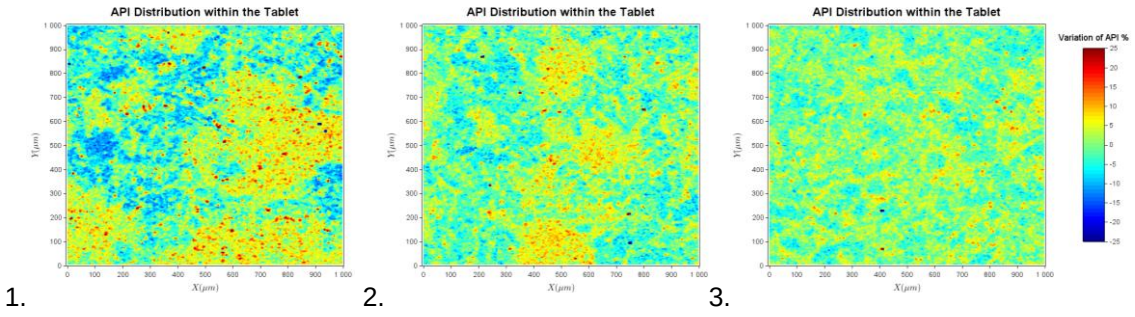

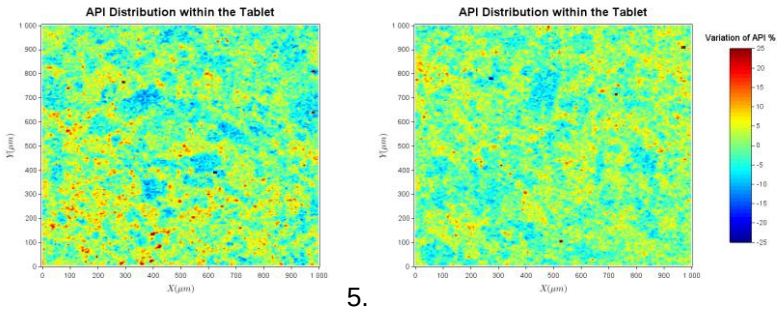

4. 5.

Figure 3.12 – API distribution within the tablet, evaluated with 5 µm of spatial resolution beneath the surface (Experiments 1, 2, 3, 4 and 5 are represented with the correspondent numbers)

The images obtained at -20 µm in depth are smoother than the ones obtained at the surface, thus overcoming the focus issue. These results prove that the Z plane evaluated can influence the results provided by CRM, as previously studied by other authors [30], [33].Additionally, histograms representing the variation of API percentage for the experiments with greater spatial resolution both at surface and under the surface are presented in Figure 3.13 and in Figure 3.14, respectively. Experiments performed under the surface presented a narrow distribution compared to the ones performed at the surface. This indicates higher level of homogeneity and corroborate the influence of focus planes studied in the obtained chemical maps.

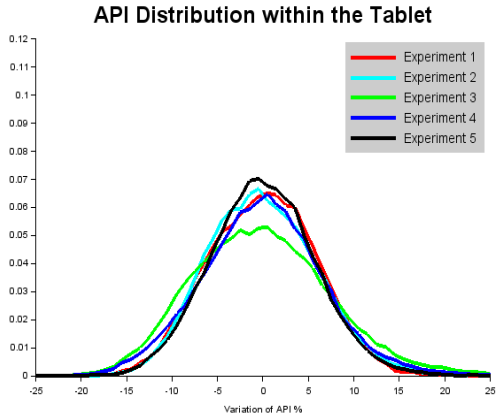

Figure 3.13 - Histogram of API% Variation at surface (Res. 5 µm)

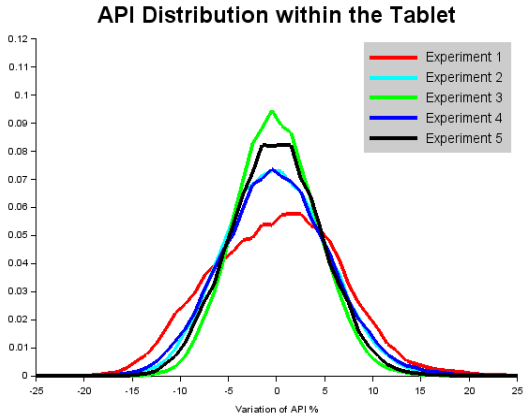

Figure 3.14 - Histogram of API% Variation under the surface (Res. 5 µm)

The Figure 3.12 shows that tablets from experiments 3, 4 and 5 did not show clusters at this spatial resolution. These experiments were produced from mixtures blended at 46 and 96 rpm and this indicates that for higher blending rotation speed, the mixtures seem to have a more homogeneous distribution, which is commonly obtained since higher blending shear induces homogeneity of the blended sample [71].

The experiments 1 and 2 showed clusters at the scale of 400 µm for the first experiment and at the scale of 200 µm for the second one. The tablets from these experiments were produced

from mixtures blended at lower rotation speed (22 rpm). So, for lower rotation speed the homogeneity of the produced tablets decreases. This result was also expected since commonly for higher blending shear the result is better homogeneity of the blended sample [71]. Counter-intuitively, this result indicates that for higher mesh size (experiment 2) smaller agglomerates are obtained (200 µm compared to 400 µm). This effect was not expected since the sieving step is performed to ensure the absence of agglomerates. Thus, for smaller sieving mesh size, the tablets would be expected to show more homogeneous distribution, since this step is known to breakdown agglomerates [67].

A possible explanation of this result could be the sieving method used during production. For the smaller mesh size (600 µm) the powder had to be forced to pass through the sieving mesh opening to perform the sieving step. Contrarily, for the larger mesh size (2000 µm) it was not necessary to force the powder against the mesh, since it flowed freely. This procedure could had induced agglomeration at the scale of the mesh opening size instead of sieving the powder for the first experiment. However, this result could not be compared with previous literature given that, to our knowledge, no author has reported a similar study in which sieving parameters were varied and the final product was studied by confocal Raman microscopy. In order to prove this theory, an additional batch could have been performed with the same conditions of the first experiment, but with the sieving step performed by vibrational techniques to avoid compressing the blend against the sieve mesh.

Additionally, the first experiment (600 µm of mesh size and 22 rpm of rotation speed) showed a broad distribution when compared to the other four experiments (Figure 3.14). This is another evidence of non-homogeneous spatial distribution at this resolution. From a previous work of Qian *et al.*, it is known that heterogeneity can be complementarily described by histograms and broader distribution corresponds to lower homogeneity [47].

In summary, chemical maps of the tablets under the surface showed possible agglomeration at a micro-scale (between 200 and 400 µm). This phenomenon was more evident for tablets made from formulations blended at a lower rotation speed (experiments 1 and 2). Larger agglomerates were found for a smaller mesh size. However, these results cannot be conclusive due to the small analyzed area (1000 µm x 1000 µm). Additional analysis under the surface could be performed in a larger area to ensure the representativeness of the sample. To understand the impact of forcing the powder to pass through the mesh, an additional batch could be performed with the sieving step executed by vibrational techniques.

Although agglomeration was detected by confocal Raman microscopy, it is important to understand if the agglomeration at a micro-scale can impact the performance of the final product. Thus, disintegration tests were conducted as surrogate for tablet performance. The test was performed in duplicate and the disintegration time for each experiment is shown in Table 3.1.

Table 3.1 - Disintegration time (in minutes) for tablets with different process parameters.

	Sieving Mesh Size (µm)			
Blending Rotation Speed (rpm)		**600**	**1000**	**2000**
	22	8.50	___	6.07
	46	___	7.72	___
	96	14.40	___	9.92

The disintegration time seems to increase with the decrease of the sieving mesh size, when the blending shear rate is maintained constant. Apart from the DoE central point, experiments 2 and 5 show decreased disintegration times (9.92 and 6.07 minutes, respectively) when compared to experiments 1 and 4 (14.40 and 8.50 minutes, respectively). This might indicate that for the formulation under study a higher mesh size could be beneficial for enhanced performance. Taking into consideration the spatial distribution of the components (Fig. 3.12 and 3.14) lower disintegration times are attributed to better spatial distribution: experiments 1 and 4 show the lowest homogeneity regarding spatial distribution of the API and the higher disintegration times (taking into account only the variation in mesh size). Although intriguing, when comparing rotation speed (keeping mesh size constant), an increase does not lead to an improvement in performance, although an improvement in spatial distribution is detected (Fig 3.14). This might indicate that, for the formulation in study, the impact of mesh size outranges the modification in rotation speed, since better disintegration times are detected for higher mesh sizes. Supporting this finding, a decrease in rotation speed sided by an increase in mesh size (experiment 3) lead to better disintegration times.

Future work concerns additional disintegration trials to enlarge the statistical relevance of this study. The faster the disintegration time, the faster the API becomes available. To evaluate the effectiveness of faster disintegration times, dissolution tests should also be conducted in the future to test the impact of faster disintegration times on API release.

4

Conclusions and Future Work

In terms of hardness characterization, the results showed an apparent relationship between the Raman spectra baseline and the measured crushing strength which was consistent with previous studies reported in the literature. However, quantitative analysis showed that the trend line was not monotonic, contrarily to the previous reports. Additionally, the slope of the trend line was comparable to the variability within the same experiment. However, these results were obtained for tablets produced from a formulation based on ASDs: a first-time study. The great variability within the same experiment could be explained by the single-point analysis. Future work concerns additional analyses performed by large area scans of the tablets' surface to ensure the representativeness of the entire sample and minimize the variability within the same experiment.

Even though the methodology studied in this work did not yield a predictive model for tablets' hardness characterization, confocal Raman microscopy was shown to be able to evaluate the sample stability during tableting. For this formulation, the API maintained its amorphous form in the range of compaction forces studied.

Concerning the spatial distribution characterization, the analysis performed with higher spatial resolution and at a few micrometers under the surface was the most suitable methodology to assess spatially resolved chemical maps. This methodology was not influenced by differences between focus planes and do not assess possible surface phenomena such as sticking and accumulation of powder at the surface. The blending shear rate and the sieving mesh size was described to impact in the distribution of components. Counter-intuitively, clusters at the scale of 400 µm were obtained for smaller mesh size. Although this effect was not expected a possible explanation could be the fact that for the smaller mesh size the powder had to be forced to pass through the mesh. This procedure could had induced agglomeration at the scale of the mesh size instead of sieving the powder for this experiment. However, this result could not be compared

with previous literature since no author has reported a similar study in which sieving parameters were varied and the final product was studied by confocal Raman microscopy. Future work concerns the evaluation of larger areas to guarantee the representativeness of the present results. On the other hand, an additional batch could have been performed with the same conditions of the first experiment, but with the sieving step performed by vibrational techniques to assess on the possible explanation given.

Lastly, the process parameters seem to have an impact on the performance of the tablets. The tablets that contained agglomerates at the micro-scale presented better performance results compared to the ones that showed a homogeneous distribution of compounds. However, these results were not conclusive since the performance tests were only conducted in duplicate. Additional disintegration trials should be performed to enlarge the statistical relevance of this study. To complement the performance characterization of the final product, dissolution in bio-relevant media should be conducted in future developments.

In conclusion, confocal Raman microscopy exhibited great potentialities for advanced characterization of ASDs, during drug product development. Additionally, confocal Raman microscopy could be combined with complementary techniques that can evaluate surface properties, such as optical profilometry or atomic force microscopy. Thus, physical and chemical properties of the tablets could be assessed by a combined advanced characterization. The future perspective is to implement and validate methods using confocal Raman microscopy for advanced characterization and formulation screening during final product development.

5

References

[1] D. Ross, “Continuous Manufacturing,” *BioPharm Int.*, vol. 28, no. 4 September, pp. 18–22, 2014.

[2] E. Sims and M. Famiglietti, “Eye on Excipients,” *Tablets & Capsules*, 2016. [Online]. Available: https://tabletscapsules.com/wp-content/uploads/pdf/tc_20160301_0047.pdf. [Accessed: 01-Sep-2018].

[3] C. Ferrero, N. Muñoz, M. V. Velasco, A. Muñoz-Ruiz, and R. Jiménez-Castellanos, “Disintegrating efficiency of croscarmellose sodium in a direct compression formulation,” *Int. J. Pharm.*, vol. 147, no. 1, pp. 11–21, Feb. 1997.

[4] R. Eyjolfsson and R. Eyjolfsson, “Introduction,” *Des. Manuf. Pharm. Tablets*, pp. 1–28, Jan. 2015.

[5] R. B. Shah, M. A. Tawakkul, and M. A. Khan, “Process Analytical Technology: Chemometric Analysis of Raman and Near Infra-red Spectroscopic Data for Predicting Physical Properties of Extended Release Matrix Tablets,” *Wiley Intersci.*, 2006.

[6] E. J. M. Meier, “Quality Aspects in Continuous Manufacturing,” in *ISPE Conference: Future Pharmaceutical Manufacturing, Continuous Manufacturing - Qualification and Validation in Practice*, 2017, no. May.

[7] C. R. Cunningham, A. Birkmire, and A. R. Rajabi-Siahboomi, “Application of a Developmental, High Productivity Film Coating in the GEA ConsiGmaTM Coater,” *AAPS 2015 poster*, p. W4177, 2015.

[8] K. Punčochová, B. Vukosavljevic, J. Hanuš, J. Beránek, M. Windbergs, and F. Štěpánek, “Non-invasive insight into the release mechanisms of a poorly soluble drug from amorphous solid dispersions by confocal Raman microscopy,” *Eur. J. Pharm. Biopharm.*, vol. 101, pp. 119–125, 2016.

[9] N. Jung and M. Windbergs, “Raman spectroscopy in pharmaceutical research and industry,” *Phys. Sci. Rev.*, p. 20170045, 2018.

[10] K. P. Cole and M. D.Johnson, “Continuous flow technology vs. the batch-by-batch approach to produce pharmaceutical compounds,” *Expert Rev. Clin. Pharmacol.*, vol. 11, pp. 5–13, 2017.

[11] J. Rantanen, “Process analytical applications of Raman spectroscopy,” *J. Pharm. Pharmacol.*, vol. 59, no. 2, pp. 171–177, 2007.

[12] K. A. Esmonde-White, M. Cuellar, C. Uerpmann, B. Lenain, and I. R. Lewis, “Raman spectroscopy as a process analytical technology for pharmaceutical manufacturing and bioprocessing,” *Anal. Bioanal. Chem.*, vol. 409, no. 3, pp. 637–649, 2017.

[13] FDA, “Guidance for Industry PAT: A Framework for Innovative Pharmaceutical Development, Manufacuring, and Quality Assurance,” *FDA Off. Doc.*, no. September, p. 16, 2004.

[14] D. Zezza, “Continuous Manufacturing : An Industry View,” in *FDA/PQRI Conference on Advancing Product Quality*, 2017.

[15] E. Peeters *et al.*, “Assessment and prediction of tablet properties using transmission and backscattering Raman spectroscopy and transmission NIR spectroscopy,” *Asian J. Pharm. Sci.*, vol. 11, no. 4, pp. 547–558, 2016.

[16] S. Wartewig and R. H. H. Neubert, “Pharmaceutical applications of Mid-IR and Raman spectroscopy,” *Adv. Drug Deliv. Rev.*, vol. 57, no. 8, pp. 1144–1170, 2005.

[17] S. Romero-Torres, J. D. Pérez-Ramos, K. R. Morris, and E. R. Grant, “Raman spectroscopic measurement of tablet-to-tablet coating variability,” *J. Pharm. Biomed. Anal.*, vol. 38, no. 2, pp. 270–274, 2005.

[18] B. W. Wabuyele, S. Sotthivirat, G. X. Zhou, J. Ash, and S. S. Dhareshwar, “Dispersive Raman Spectroscopy for Quantifying Amorphous Drug Content in Intact Tablets,” *J. Pharm. Sci.*, vol. 106, no. 2, pp. 579–588, 2017.

[19] M. J. Henson and L. Zhang, “Drug characterization in low dosage pharmaceutical tablets using raman microscopic mapping,” *Appl. Spectrosc.*, vol. 60, no. 11, pp. 1247–1255, 2006.

[20] K. Moriyama *et al.*, “Assessment of drug content uniformity of atropine sulfate triturate by liquid chromatography – tandem mass spectrometry , X-ray powder diffraction , and Raman chemical imaging,” Journal of Pharmaceutical Health Care and Sciences, 2016.

[21] M. De Veij, P. Vandenabeele, T. De Beer, J. P. Remon, and L. Moens, “Reference database of Raman spectra of pharmaceutical excipients,” *J. Raman Spectrosc.*, vol. 40, no. 3, pp. 297–307, 2009.

[22] J. Johansson, S. Pettersson, and S. Folestad, “Characterization of different laser irradiation methods for quantitative Raman tablet assessment,” *J. Pharm. Biomed. Anal.*, vol. 39, no. 3–4, pp. 510–516, 2005.

[23] S. Virtanen, O. Antikainen, and J. Yliruusi, “Determination of the crushing strength of intact tablets using Raman spectroscopy,” *Int. J. Pharm.*, vol. 360, pp. 40–46, 2008.

[24] N. Heigl *et al.*, “Potential of Raman spectroscopy for evaluating crushing strength of tablets,” *J. Pharm. Innov.*, 2012.

[25] C. R. Cunningham, A. Birkmire, and S. Gilliam, “Examinaion of Coating Process Adaptability Using Opadry QX in the GEA ConsiGmaTM Coater,” *AAPS 2016 poster*, p. 22T0130, 2016.

[26] J. Müller, D. Brock, K. Knop, J. Axel Zeitler, and P. Kleinebudde, “Prediction of dissolution time and coating thickness of sustained release formulations using Raman spectroscopy and terahertz pulsed imaging,” *Eur. J. Pharm. Biopharm.*, vol. 80, no. 3, pp. 690–697, 2012.

[27] C. Luebbert, C. Klanke, and G. Sadowski, “Investigating phase separation in amorphous solid dispersions via Raman mapping,” *Int. J. Pharm.*, vol. 535, no. 1–2, pp. 245–252, 2018.

[28] F. Tres *et al.*, “Real time Raman imaging to understand dissolution performance of amorphous solid dispersions,” *J. Control. Release*, vol. 188, no. 2014, pp. 53–60, 2014.

[29] A. Paudel, D. Raijada, and J. Rantanen, “Raman spectroscopy in pharmaceutical product design,” *Adv. Drug Deliv. Rev.*, vol. 89, pp. 3–20, 2015.

[30] T. Helešicová, T. Pekárek, and P. Matějka, “The influence of different acquisition settings and the focus adjustment on Raman spectral maps of pharmaceutical tablets,” *J. Drug Deliv. Sci. Technol.*, vol. 47, no. July, pp. 386–394, 2018.

[31] E. Smith and G. Dent, *Modern Raman Spectrocopy: A Practical Approach*. 2005.

[32] J. R. Ferraro, K. Nakamoto, and C. W. Brown, *Introductory Raman Spectroscopy*. 2003.

[33] T. Dieing, O. Hollricher, and J. Toporski, *Confocal Raman Microscopy*. Springer, 2011.

[34] G. P. S. Smith, C. M. McGoverin, S. J. Fraser, and K. C. Gordon, “Raman imaging of drug delivery systems,” *Adv. Drug Deliv. Rev.*, vol. 89, no. January, pp. 21–41, 2015.

[35] M. K. Nieuwoudt, S. E. Holroyd, C. M. McGoverin, M. C. Simpson, and D. E. Williams, “Rapid, sensitive, and reproducible screening of liquid milk for adulterants using a portable Raman spectrometer and a simple, optimized sample well,” *J. Dairy Sci.*, vol. 99, no. 10, pp. 7821–7831, 2016.

[36] R. Systems, A. Note, and K. Issues, “Raman-Based Endpoint Detection of a

Heterogeneous Etherification Reaction," 2004.

[37] Y.-S. Li and J. S. Church, "Raman spectroscopy in the analysis of food and pharmaceutical nanomaterials," *J. Food Drug Anal.*, vol. 22, no. 1, pp. 29–48, 2014.

[38] T. H. Maiman, "Ruby laser systems," US3353115A, 1961.

[39] X. Zhu, T. Xu, Q. Lin, and Y. Duan, "Technical development of raman spectroscopy: From instrumental to advanced combined technologies," *Appl. Spectrosc. Rev.*, vol. 49, no. 1, pp. 64–82, 2014.

[40] H. Eksi-Kocak, S. Ilbasmis Tamer, S. Yilmaz, M. Eryilmaz, I. H. Boyaci, and U. Tamer, "Quantification and spatial distribution of salicylic acid in film tablets using FT-Raman mapping with multivariate curve resolution," *Asian J. Pharm. Sci.*, no. 3, pp. 155–162, 2018.

[41] L. S. Taylor and F. W. Langkilde, "Evaluation of solid-state forms present in tablets by Raman spectroscopy," *J. Pharm. Sci.*, vol. 89, no. 10, pp. 1342–1353, 2000.

[42] S. Cîntă Pînzaru, I. Pavel, N. Leopold, and W. Kiefer, "Identification and characterization of pharmaceuticals using Raman and surface-enhanced Raman scattering," *J. Raman Spectrosc.*, vol. 35, no. 5, pp. 338–346, 2004.

[43] M. Jurna *et al.*, "Coherent Anti-Stokes Raman Scattering Microscopy to Monitor Drug Dissolution in Different Oral Pharmaceutical Tablets," *J. Innov. Opt. Health Sci.*, vol. 2, no. 1, pp. 37–43, 2009.

[44] J. Breitenbach, W. Schrof, and J. Neumann, "Confocal raman-spectroscopy: Analytical approach to solid dispersions and mapping of drugs," *Pharmaceutical Research*, vol. 16, no. 7. pp. 1109–1113, 1999.

[45] B. Kann and M. Windbergs, "Chemical Imaging of Drug Delivery Systems with Structured Surfaces–a Combined Analytical Approach of Confocal Raman Microscopy and Optical Profilometry," *AAPS J.*, vol. 15, no. 2, pp. 505–510, 2013.

[46] N. Scoutaris, K. Vithani, I. Slipper, B. Chowdhry, and D. Douroumis, "SEM/EDX and confocal Raman microscopy as complementary tools for the characterization of pharmaceutical tablets," *Int. J. Pharm.*, vol. 470, no. 1–2, pp. 88–98, 2014.

[47] F. Qian *et al.*, "Is a distinctive single Tga reliable indicator for the homogeneity of amorphous solid dispersion?," *Int. J. Pharm.*, vol. 395, no. 1–2, pp. 232–235, 2010.

[48] M. Marvin, "Microscopy Apparatus," US3013467A, 1957.

[49] L. Netchacovitch *et al.*, "Development of an analytical method for crystalline content determination in amorphous solid dispersions produced by hot-melt extrusion using transmission Raman spectroscopy: A feasibility study," *Int. J. Pharm.*, vol. 530, no. 1–2,

pp. 249–255, 2017.

[50] B. Li, A. Calvet, Y. Casamayou-Boucau, C. Morris, and A. G. Ryder, “Low-Content Quantification in Powders Using Raman Spectroscopy: A Facile Chemometric Approach to Sub 0.1% Limits of Detection,” *Anal. Chem.*, vol. 87, no. 6, pp. 3419–3428, 2015.

[51] United States Pharmacopeia, “RAMAN SPECTROSCOPY,” in *The United States Pharmacopeial Convention*, 2013, pp. 806–812.

[52] M. Savolainen *et al.*, “Better understanding of dissolution behaviour of amorphous drugs by in situ solid-state analysis using Raman spectroscopy,” *Eur. J. Pharm. Biopharm.*, vol. 71, no. 1, pp. 71–79, 2009.

[53] Renishaw plc, “Raman images explained.” [Online]. Available: http://www.renishaw.com/en/raman-images-explained--25810. [Accessed: 17-May-2018].

[54] R. K. May *et al.*, “Hardness and Density Distributions of Pharmaceutical Tablets Measured by Terahertz Pulsed Imaging,” *J. Pharm. Sci.*, vol. 102, no. 7, pp. 2179–2187, 2013.

[55] H. Wang, C. K. Mann, and T. J. Vickers, “Effect of powder properties on the intensity of Raman scattering by crystalline solids,” *Appl. Spectrosc.*, vol. 56, no. 12, pp. 1538–1544, 2002.

[56] S. Šašić, “An in-depth analysis of Raman and near-infrared chemical images of common pharmaceutical tablets,” *Appl. Spectrosc.*, vol. 61, no. 3, pp. 239–250, 2007.

[57] M. I. Lopes, “In vitro and in silico Dissolution and Permeation Assessment,” Universidade NOVA de Lisboa, 2017.

[58] E. Biba, “<429>LIGHT DIFFRACTION MEASUREMENT OF PARTICLE SIZE,” *United States Pharmacopeia and National Formulary (USP 41-NF 36)*, 2018. [Online]. Available: http://app.uspnf.com/uspnf/pub/index?usp=41&nf=36&s=1&officialOn=August 1, 2018.

[59] A. Shrivastava and V. Gupta, “Methods for the determination of limit of detection and limit of quantitation of the analytical methods,” *Chron Young Sci*, vol. 2, no. 1, pp. 21–25, 2011.

[60] “Tech Note: Fluorescence Limit of Detection,” *Wasatch Photonics*, 2018. [Online]. Available: https://wasatchphotonics.com/applications/fluorescence-limit-detection/. [Accessed: 10-May-2018].

[61] “<701>DISINTEGRATION,” *United States Pharmacopeia and National Formulary (USP 41-NF 36)*, 2018. [Online]. Available: http://app.uspnf.com/uspnf/pub/index?usp=41&nf=36&s=1&officialOn=August 1, 2018. [Accessed: 22-Jul-2018].

[62] F. Boukouvala, V. Niotis, R. Ramachandran, F. J. Muzzio, and M. G. Ierapetritou, “An integrated approach for dynamic flowsheet modeling and sensitivity analysis of a

continuous tablet manufacturing process," *Comput. Chem. Eng.*, vol. 42, pp. 30–47, 2012.

[63] M. Riippi, O. Antikainen, T. Niskanen, and J. Yliruusi, "The effect of compression force on surface structure, crushing strength, friability and disintegration time of erythromycin acistrate tablets," *Eur. J. Pharm. Biopharm.*, vol. 46, pp. 229–245, 1998.

[64] F. Podczeck, S. Brown, and M. Newton, "The influence of powder properties and tableting conditions on the surface roughness of tablets," *Part. Part. Syst. Charact.*, vol. 16, pp. 185–190, 1999.

[65] D. Walker, "Method and apparatus for detecting on-line homogeneity," US20030235108A1, 2001.

[66] W. E. Brown, "⟨905⟩ UNIFORMITY OF DOSAGE UNITS," *United States Pharmacopeia and National Formulary (USP 41-NF 36)*, 2018. [Online]. Available: http://app.uspnf.com/uspnf/pub/index?usp=41&nf=36&s=1&officialOn=August 1, 2018. [Accessed: 08-Aug-2018].

[67] H. Egermann, I. Kemptner, and E. Pichler, "Effects of interparticulate interactions on mixing homogeneity," *Drug Dev. Ind. Pharm.*, vol. 11, no. 2–3, pp. 663–676, 1985.

[68] D. Moonay, "What is Shear Rate and Why is it Important?," *Labcompare*, 2017. [Online]. Available: https://www.labcompare.com/10-Featured-Articles/338534-What-is-Shear-Rate-and-Why-is-it-Important/. [Accessed: 08-Feb-2018].

[69] M. Bunker, J. Zhang, R. Blanchard, and C. J. Roberts, "Characterising the surface adhesive behavior of tablet tooling components by atomic force microscopy," *Drug Dev. Ind. Pharm.*, vol. 37, no. 8, pp. 875–885, 2011.

[70] H. Garvie-Cook, K. Frederiksen, K. Petersson, R. H. Guy, and S. Gordeev, "Characterization of topical film-forming systems using atomic force microscopy and Raman microspectroscopy," *Mol. Pharm.*, vol. 12, no. 3, pp. 751–757, 2015.

[71] A. Mehrotra, M. Llusa, A. Faqih, M. Levin, and F. J. Muzzio, "Influence of shear intensity and total shear on properties of blends and tablets of lactose and cellulose lubricated with magnesium stearate," *Int. J. Pharm.*, vol. 336, no. 2, pp. 284–291, 2007.

[72] I. M. Kalogeras, "A novel approach for analyzing glass-transition temperature vs. composition patterns: Application to pharmaceutical compound + polymer systems," *Eur. J. Pharm. Sci.*, vol. 42, no. 5, pp. 470–483, 2011.

[73] E. Biba, "<941> CHARACTERIZATION OF CRYSTALLINE AND PARTIALLY CRYSTALLINE SOLIDS BY X-RAY POWDER DIFFRACTION (XRPD)," *United States Pharmacopeia and National Formulary (USP 41-NF 36)*, 2018. [Online]. Available: http://app.uspnf.com/uspnf/pub/index?usp=41&nf=36&s=1&officialOn=August 1, 2018.

6

Appendix A – ASD Characterization

First, the ASD characterization was performed by calorimetric techniques, such as TGA to evaluate the drying step efficacy and DSC to determine the glass transition temperature and also to assess the amorphous form of the powder. Then, the particle size distribution was evaluated by laser diffraction. Finally, XRPD analysis was performed to guarantee the amorphous form of the SDD, and to confirm the result given by DSC analysis. All these results are presented in this section.

TGA Analysis

For the drying step, the powder was distributed in two different trays. For this reason, the powder of each tray was analyzed by TGA to assure the efficiency of the drying. The TGA results for both the first and the second trays are presented in Figure 6.1 and Figure 6.2, respectively. The results showed no weight losses in the heating ramp analyzed. Thus, the samples showed no solvents content, demonstrating the efficacy of the drying step.

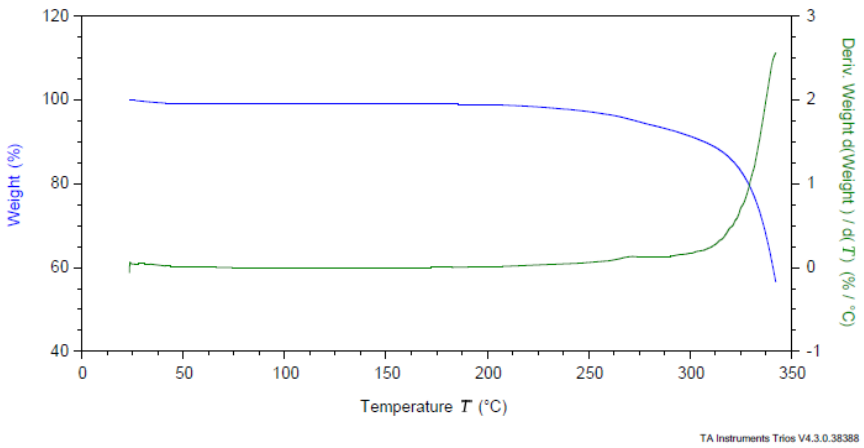

Figure 6.1 - TGA for the first tray

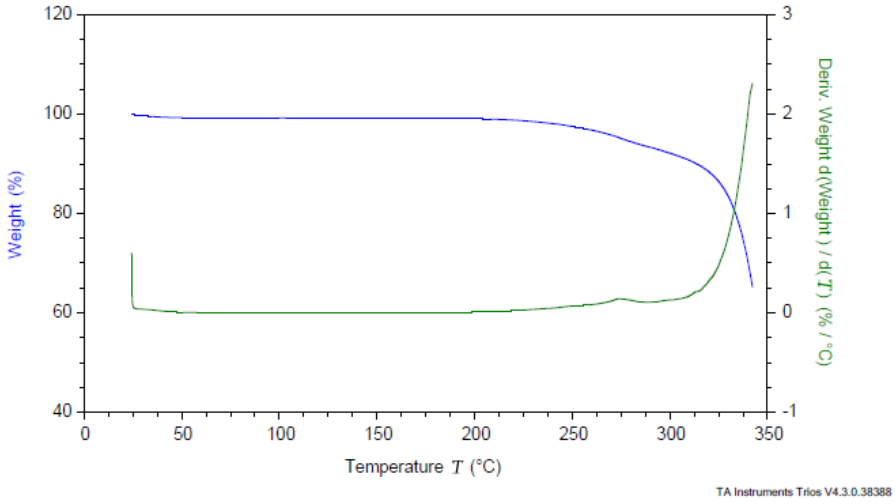

Figure 6.2 - TGA for the second tray

DSC Analysis

The DSC analysis was performed for both the determination of the glass transition temperature (Tg) and the characterization of the powder solid state. The result displayed only one Tg at 83.25 ºC, representative of the amorphous solid dispersion of Itraconazole and HPMCAS (40:60) %(w/w), as previously found in literature [72].

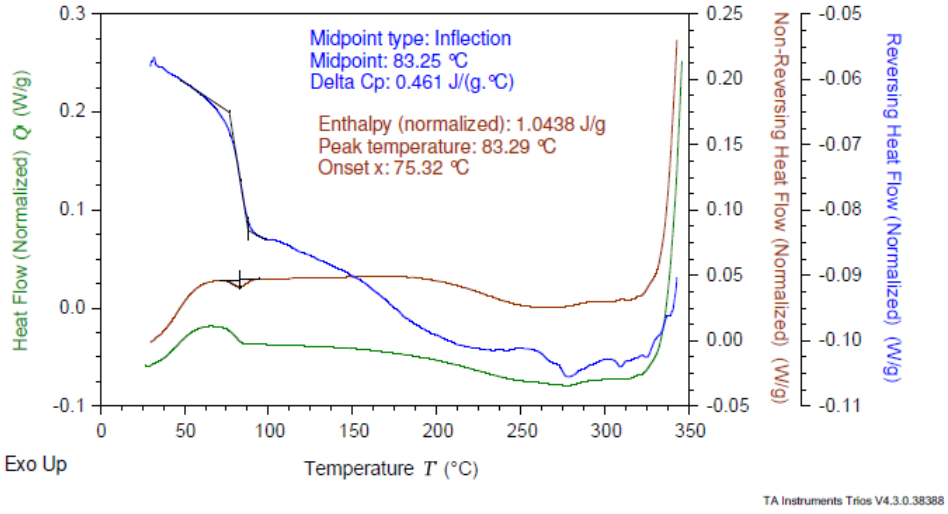

Figure 6.3 - ASD characterization by DSC

Particle Size Distribution

The ASD particle size was analyzed by laser diffraction within the range of 0.5 µm to 350 µm. The obtained central value of the distribution (Dv50) was 5.23 µm, the Dv10 and Dv90 were 1.21 and 16.58 µm, respectively. This result showed a considerable span: 2.94, comparable with the span obtained in a previous work [57]. The particle size of 5.23 µm corresponds to a value within the common range for this formulation [57].

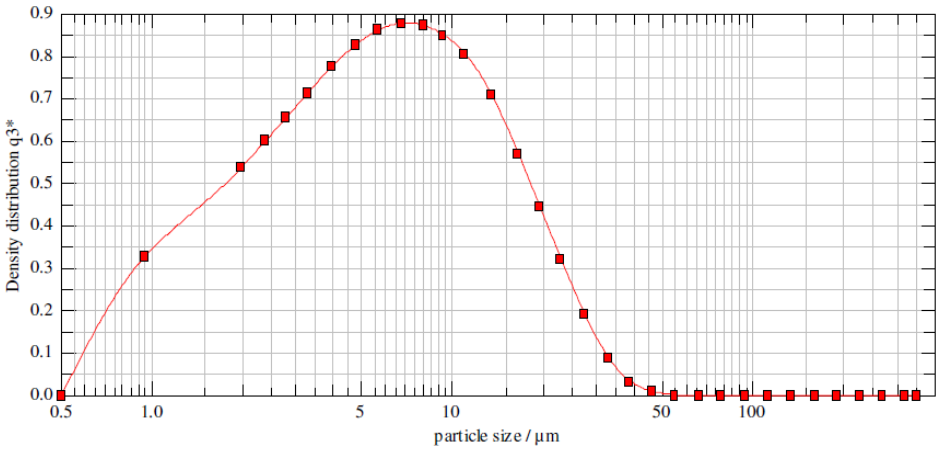

Figure 6.4 - Particle Size Distribution by Laser Diffraction

XRPD Analysis

ASD characterization by XRPD analysis was performed to determine the SDD physical form. The results showed that sharp peaks could not be observed, pointing to the amorphous form (Figure 6.5) [73].

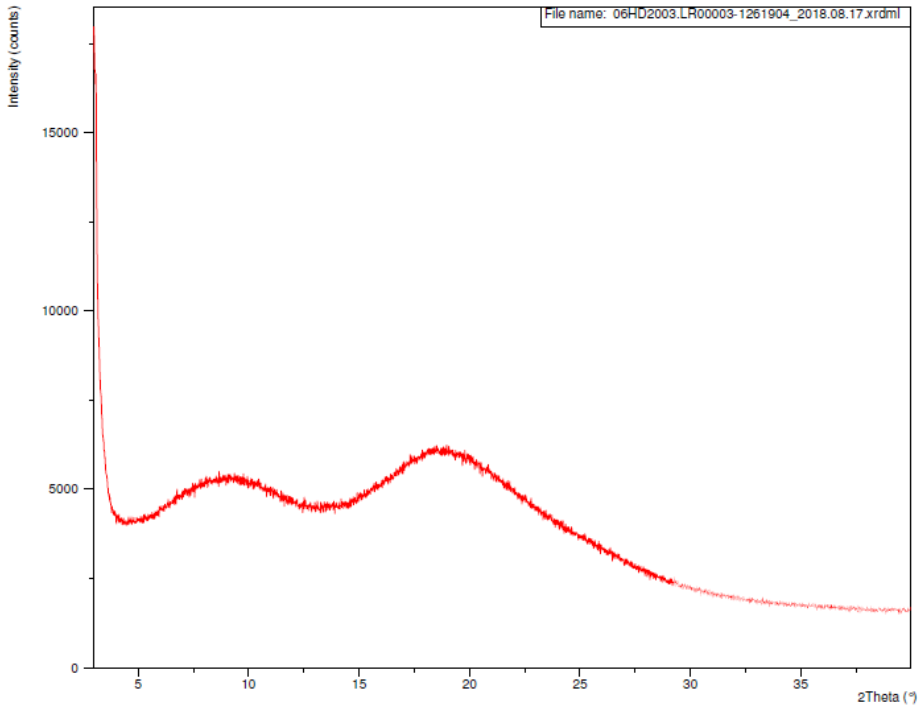

Figure 6.5 – ASD characterization by XRPD